

A block triple-relaxation-time lattice Boltzmann model for nonlinear anisotropic convection-diffusion equations

Yong Zhao^{a,b}, Yao Wu^{a,b}, Zhenhua Chai^{a,b}, Baochang Shi^{a,b,*}

^aHubei Key Laboratory of Engineering Modeling and Scientific Computing, Huazhong University of Science and Technology, Wuhan 430074, China

^bSchool of Mathematics and Statistics, Huazhong University of Science and Technology, Wuhan 430074, China

Abstract

A block triple-relaxation-time (B-TriRT) lattice Boltzmann model for general nonlinear anisotropic convection-diffusion equations (NACDEs) is proposed, and the Chapman-Enskog analysis shows that the present B-TriRT model can recover the NACDEs correctly. There are some striking features of the present B-TriRT model: firstly, the relaxation matrix of B-TriRT model is partitioned into three relaxation parameter blocks, rather than a diagonal matrix in general multiple-relaxation-time (MRT) model; secondly, based on the analysis of half-way bounce-back (HBB) scheme for Dirichlet boundary conditions, we obtain an expression to determine the relaxation parameters; thirdly, the anisotropic diffusion tensor can be recovered by the relaxation parameter block that corresponds to the first-order moment of non-equilibrium distribution function. A number of simulations of isotropic and anisotropic convection-diffusion equations are conducted to validate the present B-TriRT model. The results indicate that the present model has a second-order accuracy in space, and is also more accurate and more stable than some available lattice Boltzmann models.

Keywords: Lattice Boltzmann method, block triple-relaxation-time, nonlinear anisotropic convection-diffusion equations

1. Introduction

Lattice Boltzmann method (LBM) has now become a powerful numerical approach for simulating fluid flows and complex physical phenomena [1, 2, 3, 4, 5, 6]. Unlike conventional computational fluid dynamics (CFD) methods based on the macroscopic continuum equations, LBM is a mesoscopic kinetic-based method, and has some distinct advantages in the treatment of complex boundary and parallel computing scalability. In the past decades, LBM has gained a great success in a variety of fields, including the compressible flows [7, 8, 9, 10], heat and mass transfer in porous media [11, 12, 13, 14, 15], blood flows [16, 17, 18, 19], thermal flows [20, 21, 22, 23, 24, 25], multicomponent and multiphase flows [26, 27, 28, 29, 30, 31, 32], to name but a few. On the other hand, it also shows great potential

*Corresponding author

Email address: shibc@hust.edu.cn (Baochang Shi)

in the study of nonlinear problems, such as reaction-diffusion equation [33, 34, 35, 36], isotropic convection-diffusion equations (CDEs) [37, 38, 39, 40], anisotropic convection-diffusion equations [41, 42, 43, 44, 45, 46, 47, 48, 49], and some high-order partial differential equations [50, 51, 52, 53].

Actually, the most widely used model for nonlinear problems is lattice Bhatnagar-Gross-Krook (LBGK) model due to its high computational efficiency, but it is usually unstable for the convection-dominated problems [4]. To overcome this problem, some improved models have been proposed which can be generally grouped into two major categories: (1) the models through introducing additional parameters; (2) the models through modifying collision operator. Based on the time-splitting scheme of Boltzmann equation, Guo et al. [54] proposed a general propagation lattice Boltzmann model (GPLBM) for fluid flows. Subsequently, the model is also extended to solve nonlinear CDEs [55]. Compared to LBGK model, GPLBM can improve the numerical stability by properly adjusting two free parameters to make the Courant-Friedricks-Lewey (CFL) number smaller than 1. However, the convergence will become very slow due to the adoption of a small time-step. Recently, Xiang et al. [56] introduced a tunable parameter β to keep the dimensionless relaxation time τ away from 0.5 such that the stability of LBGK model can be improved. However, it is not convenient to choose a proper β , and the improvement of stability is not significant. Different from aforementioned models that introduce some additional parameters, a series of regularized lattice Boltzmann models (RLBMs) for fluid dynamics have also been proposed [57, 58, 59, 60]. The main idea of RLBM is to regularize the pre-collision distribution functions so as to achieve better accuracy and stability. Actually, as pointed out by Mattila [60], the regularization in LBM is a Hermite expansion of non-equilibrium distribution functions, which is used to filter the high-order non-equilibrium moments that make nonhydrodynamic contributions, so that the stability of LBM is improved. Following the similar way, Wang [61] extended the RLBM to solve nonlinear CDEs, and the results show that RLBM is more stable than traditional LBGK models. Afterward, Wang et al. also applied RLBM to investigate the fluid flows coupled with CDEs, and found that the RLBM can be written as an MRT version in [62]. In another attempt to suppress instabilities, Inamuro [63] proposed a lattice kinetic scheme (LKS) for incompressible fluid flows. In the LKS, a gradient term related to the shear rate or temperature gradient is added in the equilibrium distribution function to make the relaxation time to be unity, thus the stability of the LBM can be improved. Up to now, the LKS has been extended to some different fields [64, 65, 66, 67]. It should be noted that, the original LKS does not satisfy mass conservation law, and also destroys the localization of collision process since a finite-difference scheme is used to calculate the gradient term. To address these defects, Yang et al. [68] proposed a generalized modification lattice Boltzmann model (MLBM) for incompressible fluid flows coupled with CDEs. Different from the original LKS, Yang put the gradient term into the source term rather than equilibrium distribution function. Almost at the same time, Wang [69] et al. also proposed a modified version of LKS to guarantee the local mass conservation, and extended it to study non-newtonian fluid flows. Then, Zhao et al. [70] analyzed above two-dimensional modified

version of LKS from a mathematical point of view, and found that the modified scheme is essentially a two-relaxation-time (TRT) model. More recently, based on Chai’s work [71], Wang et al. proposed a modified LKS [72] for thermal flows. In the work, Wang et al. claimed that “the convection-diffusion equation (CDE) without the source term can be recovered with a deviation term” in MLBM, and also that “Although this deviation term can be neglected under some assumptions . . . , it still has an influence on the accuracy of the LB mode”. We would like to point out that these statements of MLBM are misunderstandings. The reason is that when the CDE is coupled with the flow field, the so-called “deviation term” in MLBM (Ref. [68], Eq. (A14)): $\partial_{t1}\phi\mathbf{u} + \lambda\nabla_1 \cdot (\phi\mathbf{u}\mathbf{u})$ can be transformed to $\phi\mathbf{a}^{(1)}$ with a $O(Ma^2)$ term being neglected reasonably. On the other hand, the treatment of the unwanted deviation term and the neglected term in Wang’s modified LKS are consistent with those in MLBM, and the numerical results presented in Ref. [72] also confirmed that. In addition, following the previous work [70], Wang et al. also performed a matrix analysis to demonstrate that both the RLBM and MLBM are TRT model essentially. After a review on the RLBM and MLBM, we would like to give some remarks: firstly, the RLBM and MLBM share similar features, but they are not included in each other; secondly, the analysis performed by Zhao et al. [70] and Wang et al. [72] are limited to two-dimensional case. In this work, we will propose a new model where RLBM and MLBM are its special cases, and extend the analysis in Ref. [70, 72] to higher-dimensional case. Furthermore, to improve the accuracy of present model, we expand the non-equilibrium distribution function to the second-order moment by Hermite polynomial, and assign a separate relaxation parameters to each Hermite components. We would like to point out the similar idea is also presented in Ref. [73]. Through a detailed matrix analysis, we demonstrated that present model can be written as a MRT form, and the relaxation parameter matrix can be partitioned into three relaxation parameter blocks. Finally, based on the analysis of HBB scheme for Dirichlet boundary conditions, we derived an expression to determine the relaxation parameters.

In addition, the LBGK models are usually limited to the isotropic CDEs since it is difficult to directly describe the anisotropic diffusion in NACDEs. To overcome the inherent defect in LBGK models, the TRT and MRT models for NACDEs are proposed by Ginzburg [42, 43, 44, 45, 46]. However, some assumptions made in Ginzburg’s models may be not satisfied for some special NACDEs [38]. Recently, Chai et al.[49] developed an MRT lattice Boltzmann model, and the general NACDEs can be correctly recovered. Although the MRT model has the ability to solve the anisotropic problems, it is not convenient to determine the free relaxation parameters, and additionally multiple-relaxation collision gives rise to more computational cost. Moreover, we also note that the anisotropic diffusion tensor is related to the first-order moment of non-equilibrium distribution function, and thus the corresponding relaxation parameter should be replaced by a matrix to describe the anisotropic diffusion tensor in NACDEs. For this reason, we utilize the relaxation parameter block that corresponds to the first-order moment of non-equilibrium distribution function to recover the anisotropic diffusion tensor.

The paper is organized as follows. In Sect. 2, the B-TriRT model for NACDEs is first presented, then a detailed Chapman-Enskog analysis is conducted. In Sect. 3, we performed a analysis of HBB scheme for Dirichlet boundary conditions to derive the relational expression to determine relaxation parameters. In Sect. 4, several numerical simulations are performed to test the accuracy and stability of present B-TriRT model, and finally some conclusions are summarized in Sect. 5. In addition, the matrix analysis is presented in Appendix.

2. The block triple-relaxation-time lattice Boltzmann model

As discussed in the Introduction, the RLBM and MLBM are developed from different points of view, but both of them can be written in a two-relaxation-time version. In this section, we will develop a B-TriRT lattice Boltzmann model, in which the RLBM and MLBM are its special cases. To see the relation between the present B-TriRT model, RLBM and MLBM, we will first present a brief introduction to the RLBM and MLBM, and then develop a B-TriRT lattice Boltzmann model.

2.1. Regularized lattice Boltzmann model

In the standard LBM, the equilibrium distribution function is projected onto a truncated Hilbert subspace \mathcal{H}_q which is spanned by a series of Hermite polynomials, while the non-equilibrium part is not. The regularization procedure work this out by projecting the relevant non-equilibrium moments onto the same subspace \mathcal{H}_q while filtering out the nonhydrodynamic moments [60]. With the aid of regularization procedure, both the equilibrium and non-equilibrium effects are limited to the subspace so that the stability of model is improved.

The evolution equation of regularized lattice Boltzmann model for CDEs reads [61]

$$f_i(\mathbf{x} + \mathbf{c}_i \Delta t, t + \Delta t) = f_i(\mathbf{x}, t) - f_i^{neq}(\mathbf{x}, t) - \left(\frac{1}{\tau} - 1 \right) \frac{\omega_i \mathbf{c}_i \cdot \sum_j \mathbf{c}_j f_j^{neq}}{c_s^2} + \Delta t G_i(\mathbf{x}, t) + \Delta t S_i(\mathbf{x}, t) + \frac{\Delta t^2}{2} D_i S_i(\mathbf{x}, t), \quad (1)$$

where $f_i(\mathbf{x}, t)$, and $f_i^{eq}(\mathbf{x}, t)$ represent the distribution function and equilibrium distribution function with the discrete velocity \mathbf{c}_i at time t in location \mathbf{x} respectively, $f_i^{neq} = f_i - f_i^{eq}$ is the non-equilibrium distribution function, τ is the dimensionless relaxation time, ω_i are the weight coefficients, c_s is the lattice sound velocity, $G_i(\mathbf{x}, \phi, t)$ is the correction term to eliminate error caused by the convection term, $S_i(\mathbf{x}, \phi, t)$ is [the distribution function of source term](#), $D_i = \partial_t + \mathbf{c}_i \cdot \nabla$ is [the gradient operator containing time and space derivatives](#).

2.2. Modified lattice Boltzmann model

The MLBM originates from LKS which is first proposed by Inamuro [63]. The main idea of LKS or MLBM is to introduce a gradient term in the equilibrium distribution function or source term to keep the relaxation time in a

proper range. In this work, we mainly focus on the MLBM, and its evolution function for CDEs can be written as

$$f_i(\mathbf{x} + \mathbf{c}_i \Delta t, t + \Delta t) = f_i - \frac{1}{\tau} f_i^{neq}(\mathbf{x}, t) - \left(\frac{1}{\tau_Z} - \frac{1}{\tau} \right) \frac{\omega_i \mathbf{c}_i \cdot \sum_j \mathbf{c}_j f_j^{neq}}{c_s^2} + \Delta t G_i + \Delta t S_i + \frac{\Delta t^2}{2} D_i S_i, \quad (2)$$

where $\tau_Z = \tau - Z$, Z is a tunable parameter.

2.3. The block triple-relaxation-time lattice Boltzmann model

Based on Eqs. (1) and (2), one can easily find that both RLBM and MLBM are specific form of the following unified evolution equation,

$$f_i(\mathbf{x} + \mathbf{c}_i \Delta t, t + \Delta t) = f_i - k_0 f_i^{neq}(\mathbf{x}, t) - (k_1 - k_0) \frac{\omega_i \mathbf{c}_i \cdot \mathbf{M}_1^{neq}(\mathbf{x}, t)}{c_s^2} + \Delta t G_i + \Delta t S_i + \frac{\Delta t^2}{2} D_i S_i, \quad (3)$$

where $\mathbf{M}_1^{neq}(\mathbf{x}, t) = \sum_j \mathbf{c}_j f_j^{neq}$ is the first-order moment of non-equilibrium distribution function f_j^{neq} , where $k_0, k_1 \in (0, 2)$ are dimensionless relaxation parameters.

In addition, in order to improve accuracy of the LB model Eq. (3), a natural idea is to expand the non-equilibrium distribution function to higher-order moments by Hermite polynomial. However, for the third-order and higher order moments, a multi-velocity lattice model is required. Hence, we only retain the second-order moment of f_i^{neq} . Then, the evolution equation of present lattice Boltzmann model reads,

$$f_i(\mathbf{x} + \mathbf{c}_i \Delta t, t + \Delta t) = f_i(\mathbf{x}, t) - k_0 f_i^{neq}(\mathbf{x}, t) - (k_1 - k_0) \frac{\omega_i \mathbf{c}_i \cdot \mathbf{M}_1^{neq}(\mathbf{x}, t)}{c_s^2} - (k_2 - k_0) \frac{\omega_i (\mathbf{c}_i \mathbf{c}_i - c_s^2 \mathbf{I}) : \mathbf{M}_2^{neq}(\mathbf{x}, t)}{2c_s^4} + \Delta t G_i(\mathbf{x}, t) + \Delta t S_i(\mathbf{x}, t) + \frac{\Delta t^2}{2} \bar{D}_i S_i(\mathbf{x}, t), \quad (4)$$

where $\mathbf{M}_2^{neq}(\mathbf{x}, t) = \sum_j \mathbf{c}_j \mathbf{c}_j f_j^{neq}$ is the second-order moment of non-equilibrium distribution function f_j^{neq} , and $\bar{D}_i = \partial_t + \gamma \mathbf{c}_i \cdot \nabla$ with γ being a tunable parameter to be determined in the following part. Furthermore, to solve some more complicated problems, (e.g., the anisotropic problems), we set the relaxation parameters k_1 and k_2 as matrices and rewrite Eq. (4) as

$$f_i(\mathbf{x} + \mathbf{c}_i \Delta t, t + \Delta t) = f_i(\mathbf{x}, t) - k_0 f_i^{neq}(\mathbf{x}, t) - \frac{\omega_i \mathbf{c}_i \cdot (\mathbf{K}_1 - k_0 \mathbf{I}) \mathbf{M}_1^{neq}(\mathbf{x}, t)}{c_s^2} - \frac{\omega_i (\mathbf{c}_i \mathbf{c}_i - c_s^2 \mathbf{I}) : (\mathbf{K}_2 - k_0 \hat{\mathbf{I}}) \circ \mathbf{M}_2^{neq}(\mathbf{x}, t)}{2c_s^4} + \Delta t G_i(\mathbf{x}, t) + \Delta t S_i(\mathbf{x}, t) + \frac{\Delta t^2}{2} \bar{D}_i S_i(\mathbf{x}, t), \quad (5)$$

where the \mathbf{K}_1 and \mathbf{K}_2 are $d \times d$ invertible and positive matrices **respectively**, with d being the spatial dimension, \mathbf{I} is an identity matrix, $\hat{\mathbf{I}}$ is a matrix with $\hat{\mathbf{I}}_{ij} = 1$, ($\forall i, j$), \circ represents the Hadamard product.

In the following, we will list some remarks on the present model:

Remark 1 : Based on a careful matrix analysis in Appendix, we can show that the evolution equation of present

B-TriRT model can be written as an MRT form,

$$f_i(\mathbf{x} + \mathbf{c}_i \Delta t, t + \Delta t) = f_i(\mathbf{x}, t) - (\mathbf{T}^{-1} \mathbf{S}_f \mathbf{T})_{ij} f_j^{neq} + \Delta t G_i + \Delta t S_i + \frac{\Delta t^2}{2} \bar{D}_i S_i, \quad (6)$$

where \mathbf{T} is the transformation matrix, and \mathbf{S}_f is the relaxation matrix, both of them are given in Appendix. In addition, we also find that the relaxation matrix \mathbf{S}_f could be partitioned into several relaxation parameter blocks as,

$$\mathbf{S}_f = \text{diag}(\mathbf{S}_0, \mathbf{S}_1, \mathbf{S}_2, \dots, \mathbf{S}_m), \quad m < q, \quad (7)$$

where m represents the order of moment, q represents the number of discrete velocities. Based on the concept of block, the general multiple-relaxation-time could be extended to a block multiple-relaxation-time version. Actually, as mentioned above, for the third-order and higher-order moments, a multi-velocity model is required. For this reason, we only partition the relaxation matrix into three relaxation parameter blocks as: \mathbf{S}_0 , \mathbf{S}_1 and \mathbf{S}_2 , the model is also named B-TriRT model, where $\mathbf{S}_1 = \mathbf{K}_1$ that corresponds to the first-order moment of non-equilibrium distribution function, \mathbf{S}_2 is related to \mathbf{K}_2 that corresponds to second-order moment of non-equilibrium distribution function, $\mathbf{S}_0 = k_0 \mathbf{I}$ that corresponds to the remaining moments of non-equilibrium distribution function. In addition, the present B-TriRT model can also be reduced to TRT model in Ref. [74, 75] by setting $\mathbf{K}_2 = k_0 \hat{\mathbf{I}}$ for the $DdQq$, $q = 2d$ or $2d + 1$ lattice model. However, for general $DdQq$, $q \neq 2d$ or $2d + 1$ lattice model, the TRT model cannot be categorized into the present B-TriRT model.

Remark II : The RLBM and MLBM are special cases of the present B-TriRT model. By adopting the relaxation parameters $\mathbf{K}_1 = k_1 \mathbf{I}$, $\mathbf{K}_2 = k_2 \hat{\mathbf{I}}$, and choosing appropriate parameters k_1 , k_2 , we can obtain the LBGK model, RLBM and MLBM from present model, as seen from Tab. 1.

Table 1: Parameter values corresponding to different models

Model	k_0	k_1	k_2
LBGK	$1/\tau$	$1/\tau$	$1/\tau$
MLBM	$1/\tau$	$1/\tau_Z$	$1/\tau$
RLBM	1	$1/\tau$	1

Remark III : As pointed out by Chai et al. [49], there are two special schemes to treat the source term derivative $\bar{D}_i S_i(\mathbf{x}, t)$ in evolution equation based on the choice of the parameter γ .

Schemes 1 ($\gamma = 1$) : In this scheme, both the time and space derivatives are contained in the evolution equation. However, when we use the finite-difference scheme to calculate the space derivative, the collision process cannot be conducted locally. Although, we can adopt some spacial technologies as mentioned in [49] to maintain the locality of computation, it brings more matrix multiplication which will reduce the computational efficiency.

Schemes 2 ($\gamma = 0$) : In the second scheme, the derivative term $\bar{D}_t S_i(\mathbf{x}, t)$ would reduce to $\partial_t S_i(\mathbf{x}, t)$, and an explicit finite-difference scheme (i.e., $\partial_t S_i(\mathbf{x}, t) = [S_i(\mathbf{x}, t) - S_i(\mathbf{x}, t - \delta t)]/\delta t$) is applied to compute the time derivative. In the present model, we adopt the second scheme ($\gamma = 0$) to compute the source term derivative $\bar{D}_t S_i(\mathbf{x}, t)$ for simplicity, and it can also be implemented locally.

Remark IV : We would like to point out that the present B-TriRT model can be adopted to solve both NACDEs and Navier-Stokes equations (NSEs). For NACDEs, the relaxation parameter \mathbf{K}_1 is related to the diffusion term, while for NSEs, \mathbf{K}_1 can be set arbitrary since the first-order moment of non-equilibrium distribution function is equal to zero based on momentum conservation law, and the relaxation parameter \mathbf{K}_2 is related to the viscous term. However, in this work, we mainly focus on the NACDEs,

$$\partial_t \phi + \nabla \cdot \mathbf{B}(\mathbf{x}, \phi, t) = \nabla \cdot [\mathbf{A}(\mathbf{x}, \phi, t) \nabla \cdot \mathbf{D}(\mathbf{x}, \phi, t)] + S(\mathbf{x}, \phi, t), \quad (8)$$

where ϕ is the scalar variable and is a function of space \mathbf{x} and time t , ∇ is the gradient operator, $\mathbf{B}(\mathbf{x}, \phi, t)$, $\mathbf{D}(\mathbf{x}, \phi, t)$ and $S(\mathbf{x}, \phi, t)$ are the known convection term, diffusion term and source term. $\mathbf{A}(\mathbf{x}, t)$ is the diffusion tensor, it can also be the function of scalar variable ϕ , space \mathbf{x} and time t .

2.4. The B-TriRT model for NACDEs

In the B-TriRT model for NACDEs, the equilibrium distribution function $f_i^{eq}(\mathbf{x}, t)$ is given as

$$f_i^{eq}(\mathbf{x}, t) = \omega_i \left[\phi + \frac{\mathbf{c}_i \cdot \mathbf{B}(\mathbf{x}, \phi, t)}{c_s^2} + \frac{(\mathbf{D}(\mathbf{x}, \phi, t) - \phi \mathbf{I}) : (\mathbf{c}_i \mathbf{c}_i - c_s^2 \mathbf{I})}{2c_s^2} \right], \quad (9)$$

and the [distribution function of source term](#) reads

$$S_i^{eq}(\mathbf{x}, t) = \omega_i S(\mathbf{x}, t). \quad (10)$$

Based on Eqs. (9, 10), one can obtain the following conditions,

$$\sum_i f_i = \sum_i f_i^{eq} = \phi, \quad \sum_i \mathbf{c}_i f_i^{eq} = \mathbf{B}(\mathbf{x}, \phi, t), \quad \sum_i \mathbf{c}_i \mathbf{c}_i f_i^{eq} = c_s^2 \mathbf{D}(\mathbf{x}, \phi, t), \quad (11)$$

$$\sum_i S_i = S(\mathbf{x}, \phi, t), \quad \sum_i \mathbf{c}_i S_i = 0. \quad (12)$$

The correction term $G_i(\mathbf{x}, \phi, t)$ in Eq.(5) is used to eliminate the additional term caused by convection term (i.e., $\nabla \cdot \partial_t \mathbf{B}(\mathbf{x}, \phi, t)$, see the details in the Chapman-Enskog analysis), and is defined as

$$G_i(\mathbf{x}, \phi, t) = \frac{\omega_i \mathbf{c}_i \cdot \left(\mathbf{I} - \frac{\mathbf{K}_1}{2} \right) \partial_t \mathbf{B}(\mathbf{x}, \phi, t)}{c_s^2}. \quad (13)$$

In the following part, we will perform a detailed Chapman-Enskog analysis to recover the macroscopic equation (8) from evolution equation (5). Firstly, we expand the distribution function, the time and space derivatives as

$$\begin{aligned} f_i &= f_i^{(0)} + \varepsilon f_i^{(1)} + \varepsilon^2 f_i^{(2)} + \dots, \\ \mathbf{M}_r^{neq} &= \mathbf{M}_r^{neq(0)} + \varepsilon \mathbf{M}_r^{neq(1)} + \varepsilon^2 \mathbf{M}_r^{neq(2)}, \quad r = 1, 2, \\ \mathbf{M}_1^{neq(0)} &= \sum_i \mathbf{c}_i (f_i^{(0)} - f_i^{eq}), \\ \mathbf{M}_2^{neq(0)} &= \sum_i \mathbf{c}_i \mathbf{c}_i (f_i^{(0)} - f_i^{eq}), \\ \mathbf{M}_1^{neq(l)} &= \sum_i \mathbf{c}_i f_i^{(l)}, \quad l = 1, 2 \\ \mathbf{M}_2^{neq(l)} &= \sum_i \mathbf{c}_i \mathbf{c}_i f_i^{(l)}, \quad l = 1, 2 \\ S_i &= \varepsilon S_i^{(1)}, \\ G_i &= \varepsilon G_i^{(1)} + \varepsilon^2 G_i^{(2)}, \\ \partial_t &= \varepsilon \partial_{t1} + \varepsilon^2 \partial_{t2}, \\ \nabla &= \varepsilon \nabla_1. \end{aligned} \quad (14)$$

Applying the Taylor series expansion to the evolution equation Eq. (5) at time t and position \mathbf{x} , we have

$$\begin{aligned} \Delta t D_i f_i + \frac{\Delta^2}{2} D_i^2 f_i + \dots &= -k_0 f_i^{neq} - \frac{\omega_i \mathbf{c}_i \cdot (\mathbf{K}_1 - k_0 \mathbf{I}) \mathbf{M}_1^{neq}(\mathbf{x}, t)}{c_s^2} - \frac{\omega_i (\mathbf{c}_i \mathbf{c}_i - c_s^2 \mathbf{I}) : (\mathbf{K}_2 - k_0 \hat{\mathbf{I}}) \circ \mathbf{M}_2^{neq}(\mathbf{x}, t)}{2c_s^4} \\ &+ \Delta t G_i(\mathbf{x}, t) + \Delta t S_i(\mathbf{x}, t) + \frac{\Delta t^2}{2} \bar{D}_i S_i(\mathbf{x}, t), \end{aligned} \quad (15)$$

Substituting Eq. (14) into Eq. (15), one can obtain:

$$\begin{aligned}
& \Delta t(\varepsilon D_{1i} + \varepsilon^2 \partial_{t2})(f_i^{(0)} + \varepsilon f_i^{(1)} + \varepsilon^2 f_i^{(2)}) + \frac{\Delta t^2}{2}(\varepsilon D_{1i} + \varepsilon^2 \partial_{t2})^2(f_i^{(0)} + \varepsilon f_i^{(1)} + \varepsilon^2 f_i^{(2)}) \\
& = -k_0(f_i^{(0)} + \varepsilon f_i^{(1)} + \varepsilon^2 f_i^{(2)} - f_i^{eq}) - \frac{\omega_i \mathbf{c}_i \cdot (\mathbf{K}_1 - k_0 \mathbf{I})(\mathbf{M}_1^{neq(0)} + \varepsilon \mathbf{M}_1^{neq(1)} + \varepsilon^2 \mathbf{M}_1^{neq(2)})}{c_s^2} \\
& \quad - \frac{\omega_i(\mathbf{c}_i \mathbf{c}_i - c_s^2 \mathbf{I}) : (\mathbf{K}_2 - k_0 \hat{\mathbf{I}}) \circ (\mathbf{M}_2^{neq(0)} + \varepsilon \mathbf{M}_2^{neq(1)} + \varepsilon^2 \mathbf{M}_2^{neq(2)})}{2c_s^4} + \Delta t(\varepsilon G_i^{(1)} + \varepsilon^2 G_i^{(2)}) + \Delta t \varepsilon S_i^{(1)} + \frac{\Delta t^2}{2}(\varepsilon^2 \bar{D}_{1i} + \varepsilon^3 \partial_{t2})S_i^{(1)}.
\end{aligned} \tag{16}$$

where $D_{1i} = \partial_{t1} + \mathbf{c}_i \cdot \nabla_1$, $\bar{D}_{1i} = \partial_{t1} + \gamma \mathbf{c}_i \cdot \nabla_1$.

Based on Eq. (16), one can derive the following equations at different orders of ε :

$$O(\varepsilon^0) : k_0(f_i^{(0)} - f_i^{eq}) + \frac{\omega_i \mathbf{c}_i \cdot (\mathbf{K}_1 - k_0 \mathbf{I}) \mathbf{M}_1^{neq(0)}}{c_s^2} - \frac{\omega_i(\mathbf{c}_i \mathbf{c}_i - c_s^2 \mathbf{I}) : (\mathbf{K}_2 - k_0 \hat{\mathbf{I}}) \circ \mathbf{M}_2^{neq(0)}}{2c_s^4} = 0, \tag{17}$$

$$O(\varepsilon^1) : \Delta t D_{1i} f_i^{(0)} = -k_0 f_i^{(1)} - \frac{\omega_i \mathbf{c}_i \cdot (\mathbf{K}_1 - k_0 \mathbf{I}) \mathbf{M}_1^{neq(1)}}{c_s^2} - \frac{\omega_i(\mathbf{c}_i \mathbf{c}_i - c_s^2 \mathbf{I}) : (\mathbf{K}_2 - k_0 \hat{\mathbf{I}}) \circ \mathbf{M}_2^{neq(1)}}{2c_s^4} + \Delta t S_i^{(1)} + \Delta t G_i^{(1)}, \tag{18}$$

$$O(\varepsilon^2) : \Delta t D_{1i} f_i^{(1)} + \Delta t \partial_{t2} f_i^{(0)} + \frac{\Delta t^2}{2} D_{1i}^2 f_i^{(0)} = -k_0 f_i^{(2)} - \frac{\omega_i \mathbf{c}_i \cdot (\mathbf{K}_1 - k_0 \mathbf{I}) \mathbf{M}_1^{neq(2)}}{c_s^2} - \frac{\omega_i(\mathbf{c}_i \mathbf{c}_i - c_s^2 \mathbf{I}) : (\mathbf{K}_2 - k_0 \hat{\mathbf{I}}) \circ \mathbf{M}_2^{neq(2)}}{2c_s^4} + \Delta t G_i^{(2)} + \frac{\Delta t^2}{2} \bar{D}_{1i} S_i^{(1)} \tag{19}$$

Multiplying Eq. (17) by \mathbf{c}_i and $\mathbf{c}_i \mathbf{c}_i$, then summing them over i , we get

$$\mathbf{K}_1 \mathbf{M}_1^{neq(0)} = 0, \quad \mathbf{K}_2 \circ \mathbf{M}_2^{neq(0)} = 0, \tag{20}$$

based on the fact that \mathbf{K}_1 is invertible and \mathbf{K}_2 consists of non-zero elements, one can obtain the following conclusion:

$$\mathbf{M}_1^{neq(0)} = 0, \quad \mathbf{M}_2^{neq(0)} = 0. \tag{21}$$

Substituting Eq. (21) into Eq. (17) yields

$$k_0(f_i^{(0)} - f_i^{eq}) = 0, \tag{22}$$

which also leads to

$$f_i^{(0)} = f_i^{eq}. \tag{23}$$

Then from Eqs. (11), (14) and (23), one can easily obtain

$$\sum_i f_i^{(n)} = 0, n \geq 1. \tag{24}$$

With the help of Eq. (18), we can rewrite the Eq. (19) as

$$\begin{aligned} & \Delta t D_{1i} f_i^{(1)} + \Delta t \partial_{t2} f_i^{(0)} + \frac{\Delta t}{2} D_{1i} \left(-k_0 f_i^{(1)} - \frac{\omega_i \mathbf{c}_i \cdot (\mathbf{K}_1 - k_0 \mathbf{I}) \mathbf{M}_1^{neq(1)}}{c_s^2} - \frac{\omega_i (\mathbf{c}_i \mathbf{c}_i - c_s^2 \mathbf{I}) : (\mathbf{K}_2 - k_0 \hat{\mathbf{I}}) \circ \mathbf{M}_2^{neq(1)}}{2c_s^4} + \Delta t G_i^{(1)} + \Delta t S_i^{(1)} \right) \\ & = -k_0 f_i^{(2)} - \frac{\omega_i \mathbf{c}_i \cdot (\mathbf{K}_1 - k_0 \mathbf{I}) \mathbf{M}_1^{neq(2)}}{c_s^2} - \frac{\omega_i (\mathbf{c}_i \mathbf{c}_i - c_s^2 \mathbf{I}) : (\mathbf{K}_2 - k_0 \hat{\mathbf{I}}) \circ \mathbf{M}_2^{neq(2)}}{2c_s^4} + \Delta t G_i^{(2)} + \frac{\Delta t^2}{2} \bar{D}_{1i} S_i^{(1)}. \end{aligned} \quad (25)$$

Rearrange the Eq.(25), we have

$$\begin{aligned} & \Delta t D_{1i} \left(1 - \frac{k_0}{2} \right) f_i^{(1)} + \Delta t \partial_{t2} f_i^{(0)} - \frac{\Delta t}{2} D_{1i} \left(\frac{\omega_i \mathbf{c}_i \cdot (\mathbf{K}_1 - k_0 \mathbf{I}) \mathbf{M}_1^{neq(1)}}{c_s^2} + \frac{\omega_i (\mathbf{c}_i \mathbf{c}_i - c_s^2 \mathbf{I}) : (\mathbf{K}_2 - k_0 \hat{\mathbf{I}}) \circ \mathbf{M}_2^{neq(1)}}{2c_s^4} - \Delta t G_i^{(1)} \right) \\ & = -k_0 f_i^{(2)} - \frac{\omega_i \mathbf{c}_i \cdot (\mathbf{K}_1 - k_0 \mathbf{I}) \mathbf{M}_1^{neq(2)}}{c_s^2} - \frac{\omega_i (\mathbf{c}_i \mathbf{c}_i - c_s^2 \mathbf{I}) : (\mathbf{K}_2 - k_0 \hat{\mathbf{I}}) \circ \mathbf{M}_2^{neq(2)}}{2c_s^4} + \Delta t G_i^{(2)} + \frac{\Delta t^2}{2} (\bar{D}_{1i} - D_{1i}) S_i^{(1)}. \end{aligned} \quad (26)$$

Summing Eqs. (18) and (26) over i , and utilizing Eqs. (9), (10), (11), (24), one can derive the following equations,

$$\partial_{t1} \phi + \nabla_1 \cdot \mathbf{B}(\mathbf{x}, \phi, t) = S^{(1)}, \quad (27)$$

$$\partial_{t2} \phi + \nabla_1 \cdot \left(\mathbf{I} - \frac{\mathbf{K}_1}{2} \right) \sum_i \mathbf{c}_i f_i^{(1)} + \frac{\Delta t}{2} \nabla \cdot \left(\mathbf{I} - \frac{\mathbf{K}_1}{2} \right) \partial_{t1} \mathbf{B}(\mathbf{x}, \phi, t) = 0. \quad (28)$$

Multiplying Eq.(18) by \mathbf{c}_i and summing it over i , it is easy to get

$$\begin{aligned} \mathbf{K}_1 \sum_i \mathbf{c}_i f_i^{(1)} & = -\Delta t \left(\partial_{t1} \sum_i \mathbf{c}_i f_i^{(0)} + \nabla_1 \cdot \sum_i \mathbf{c}_i \mathbf{c}_i f_i^{(0)} \right) + \Delta t \sum_i \mathbf{c}_i G_i^{(1)} \\ & = -\Delta t \left[\partial_{t1} \mathbf{B}(\mathbf{x}, \phi, t) + \nabla_1 \cdot c_s^2 \mathbf{D}(\mathbf{x}, \phi, t) \right] + \Delta t \left(\mathbf{I} - \frac{\mathbf{K}_1}{2} \right) \partial_{t1} \mathbf{B}(\mathbf{x}, \phi, t) \\ & = -\Delta t \nabla_1 \cdot c_s^2 \mathbf{D}(\mathbf{x}, \phi, t) - \Delta t \frac{\mathbf{K}_1}{2} \partial_{t1} \mathbf{B}(\mathbf{x}, \phi, t). \end{aligned} \quad (29)$$

Multiplying Eq.(29) by \mathbf{K}_1^{-1} , and substituting the result into Eq. (28) yields

$$\partial_{t2} \phi = \nabla_1 \cdot \left[c_s^2 \left(\mathbf{K}_1^{-1} - \frac{1}{2} \mathbf{I} \right) \Delta t \nabla_1 \cdot \mathbf{D}(\mathbf{x}, \phi, t) \right]. \quad (30)$$

Applying Eq. (28) $\times \varepsilon$ + Eq. (30) $\times \varepsilon^2$, we can recover the NACDE

$$\partial_t \phi + \nabla \cdot \mathbf{B}(\mathbf{x}, \phi, t) = \nabla \cdot [\mathbf{A}(\mathbf{x}, \phi, t) \nabla \cdot \mathbf{D}(\mathbf{x}, \phi, t)] + S(\mathbf{x}, \phi, t), \quad (31)$$

with

$$\mathbf{A}(\mathbf{x}, \phi, t) = c_s^2 \left(\mathbf{K}_1^{-1} - \frac{1}{2} \mathbf{I} \right) \Delta t. \quad (32)$$

3. Analysis of HBB scheme for Dirichlet boundary conditions

In this section, we will conduct a analysis of HBB scheme for Dirichlet boundary conditions to derive a relation between \mathbf{K}_1 and \mathbf{K}_2 . Here we take a unidirectional steady diffusion problem as an example, which can be described by [76]

$$\partial_t \phi + \nabla \cdot (\phi \mathbf{u}) = \nabla \cdot (\alpha \nabla \phi) + S, \quad (33)$$

$$\phi(t, x, 0) = \phi_0, \quad \phi(t, x, L) = \phi_L, \quad (34)$$

where $\mathbf{u} = (u_x, 0)^T$ with u_x being a constant, α is a constant diffusion coefficient, $S = 2\alpha\Delta\phi/L^2$ is the source term with $\Delta\phi = \phi_L - \phi_0$. One can easily derive its analytical solution,

$$\phi(x, y) = \phi_0 + \Delta\phi y(2 - y). \quad (35)$$

To obtain the numerical solution of this problem, we first give the equivalent difference equation of present model. Since this example is an unidirectional steady diffusion problem, and the source term S is a constant, we can adopt the following linear equilibrium distribution function,

$$f_i^{eq}(\mathbf{x}, t) = \omega_i \phi \left(1 + \frac{\mathbf{c}_i \cdot \mathbf{u}}{c_s^2} \right), \quad (36)$$

and the evolution equation is composed of the collision and propagation steps,

$$f_i^+(\mathbf{x}, t) = f_i(\mathbf{x}, t) - (\mathbf{T}^{-1} \mathbf{S}_f \mathbf{T})_{ij} f_j^{neq} + \Delta t \omega_i S, \quad f_i(\mathbf{x} + \mathbf{c}_i \Delta t, t + \Delta t) = f_i^+(\mathbf{x}, t), \quad (37)$$

where the superscript “+” means post-collision. Here we employ the popular D2Q9 lattice model for the problem and the weight coefficients are given as $\omega_0 = 4/9$, $\omega_{1,2,3,4} = 1/9$, $\omega_{5,6,7,8} = 1/36$. For this lattice model, we can obtain the following equations from Eqs. (36)-(37),

$$\begin{aligned} f_0^n + f_1^n + f_3^n = & f_0^n + f_1^n + f_3^n - k_0 \left[f_0^n + f_1^n + f_3^n - (f_0^{n,eq} + f_1^{n,eq} + f_3^{n,eq}) \right] \\ & - (k_0 - k_2) \left[f_2^n + f_4^n + f_5^n + f_6^n + f_7^n + f_8^n - (f_2^{n,eq} + f_4^{n,eq} + f_5^{n,eq} + f_6^{n,eq} + f_7^{n,eq} + f_8^{n,eq}) \right] + \frac{2}{3} \Delta t S, \end{aligned} \quad (38)$$

$$f_2^{n+1} + f_5^{n+1} + f_6^{n+1} = f_2^n + f_5^n + f_6^n - \left(\frac{k_1}{2} + \frac{k_2}{2}\right) [f_2^n + f_5^n + f_6^n - (f_2^{n,eq} + f_5^{n,eq} + f_6^{n,eq})] - \left(\frac{k_2}{2} - \frac{k_1}{2}\right) [f_4^n + f_7^n + f_8^n - (f_4^{n,eq} + f_7^{n,eq} + f_8^{n,eq})] + \frac{1}{3}\Delta t S, \quad (39)$$

$$f_4^{n-1} + f_7^{n-1} + f_8^{n-1} = f_4^n + f_7^n + f_8^n - \left(\frac{k_2}{2} - \frac{k_1}{2}\right) [f_2^n + f_5^n + f_6^n - (f_2^{n,eq} + f_5^{n,eq} + f_6^{n,eq})] - \left(\frac{k_1}{2} + \frac{k_2}{2}\right) [f_4^n + f_7^n + f_8^n - (f_4^{n,eq} + f_7^{n,eq} + f_8^{n,eq})] + \frac{1}{3}\Delta t S, \quad (40)$$

where f_i^n is the distribution function at the layer n in the y direction.

Based on the Eqs. (11) and (36), we can rewrite the Eq. (38) as

$$f_0^n + f_1^n + f_3^n = \frac{2}{3}\phi_n + \frac{2}{3k_2}\Delta t S, \quad (41)$$

then according to Eq. (12), we also have

$$(f_2^n + f_5^n + f_6^n) + (f_4^n + f_7^n + f_8^n) = \frac{1}{3}\phi_n - \frac{2}{3k_2}\Delta t S. \quad (42)$$

Substituting Eq. (42) into Eq. (39) and Eq. (40) yields

$$f_2^{n+1} + f_5^{n+1} + f_6^{n+1} = \frac{2-k_1}{6}\phi_n + \frac{k_1}{2c}\phi_n u_{y,n} + (k_1-1)(f_4^n + f_7^n + f_8^n) + \frac{1}{6}\Delta t S - \left(1 - \frac{k_1}{2} - \frac{k_2}{2}\right) \frac{2}{3k_2}\Delta t S, \quad (43)$$

$$f_4^{n-1} + f_7^{n-1} + f_8^{n-1} = \frac{2-k_1}{6}\phi_n + \frac{k_1}{2c}\phi_n u_{y,n} + (k_1-1)(f_2^n + f_5^n + f_6^n) + \frac{1}{6}\Delta t S - \left(1 - \frac{k_1}{2} - \frac{k_2}{2}\right) \frac{2}{3k_2}\Delta t S. \quad (44)$$

Based on Eqs. (43) and (44), we can obtain the following equations,

$$f_2^n + f_5^n + f_6^n = \frac{2-k_1}{6}\phi_{n-1} + (k_1-1)(f_4^{n-1} + f_7^{n-1} + f_8^{n-1}) + \frac{k_1}{2c}\phi_{n-1} u_{y,n-1} + \frac{1}{6}\Delta t S - \left(1 - \frac{k_1}{2} - \frac{k_2}{2}\right) \frac{2}{3k_2}\Delta t S \quad (45)$$

$$f_4^n + f_7^n + f_8^n = \frac{2-k_1}{6}\phi_{n+1} + (k_1-1)(f_2^{n+1} + f_5^{n+1} + f_6^{n+1}) + \frac{k_1}{2c}\phi_{n+1} u_{y,n+1} + \frac{1}{6}\Delta t S - \left(1 - \frac{k_1}{2} - \frac{k_2}{2}\right) \frac{2}{3k_2}\Delta t S. \quad (46)$$

A summation of Eq. (45) and Eq. (46), and with aid of Eqs. (43) and (44), we can derive the equivalent difference equation of present model as

$$\frac{\phi_{n+1} u_{y,n+1} - \phi_{n-1} u_{y,n-1}}{2\Delta x} = \alpha \frac{\phi_{n-1} - 2\phi_n + \phi_{n+1}}{\Delta x^2} + S. \quad (47)$$

where the diffusion coefficient α is given by Eq. (32) with $c_s^2 = c^2/3$.

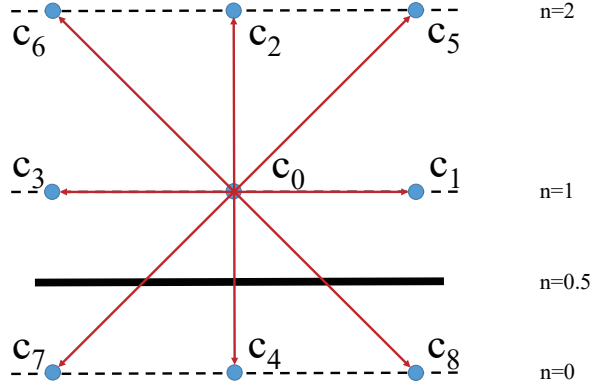


Figure 1: The half-way bounce back scheme in D2Q9 lattice model; the solid line denotes the bottom physical boundary while the dotted line denotes the computational grid.

By adopting a HBB scheme for Dirichlet boundary conditions [77], as shown in Fig. 1, Eq. (47) has a simple solution:

$$\phi_n = \phi_0 + \Delta\phi y_n(2 - y_n) + \phi_s, \quad (48)$$

where $y_n = (n - 1/2)/N$ with N denoting the grid number in y direction, ϕ_s represents the *numerical slip* caused by the discrete effect of boundary condition [78, 76].

We now turn to derive the *numerical slip* by conducting some algebraic manipulations. From Eq. (48), we can get

$$\phi_1 = \phi_0 + \frac{1}{2N} \left(2 - \frac{1}{2N} \right) + \phi_s, \quad (49)$$

$$\phi_2 = \phi_0 + \frac{3}{2N} \left(2 - \frac{3}{2N} \right) + \phi_s. \quad (50)$$

With the help of the $u_x = 0.1, u_y = 0$, substituting Eq. (45) into Eq. (44) yields

$$\begin{aligned} f_4^{n-1} + f_7^{n-1} + f_8^{n-1} = & \frac{2 - k_1}{6} \phi_n + (k_1 - 1) \left[\frac{2 - k_1}{6} \phi_{n-1} + (k_1 - 1)(f_4^{n-1} + f_7^{n-1} + f_8^{n-1}) + \frac{1}{6} \Delta t S - \left(1 - \frac{k_1}{2} - \frac{k_2}{2} \right) \frac{2}{3k_2} \Delta t S \right] \\ & + \frac{1}{6} \Delta t S - \left(1 - \frac{k_1}{2} - \frac{k_2}{2} \right) \frac{2}{3k_2} \Delta t S \end{aligned} \quad (51)$$

rearranging above equation, we have

$$k_1(f_4^{n-1} + f_7^{n-1} + f_8^{n-1}) = \frac{1}{6} \phi_n + \frac{k_1 - 1}{6} \phi_{n-1} + \frac{s_1}{2 - k_1} \left[\frac{1}{6} \Delta t S - \left(1 - \frac{k_1}{2} - \frac{k_2}{2} \right) \frac{2}{3k_2} \Delta t S \right] \quad (52)$$

Based on HBB scheme, one can obtain

$$f_2^1 = -f_4^{1,+} + 2w_4\phi_0, \quad (53)$$

$$f_5^1 = -f_7^{1,+} + 2w_7\phi_0, \quad (54)$$

$$f_6^1 = -f_8^{1,+} + 2w_8\phi_0. \quad (55)$$

After a summation of Eqs. (53)-(55), we have

$$f_2^1 + f_5^1 + f_6^1 = -(f_4^{1,+} + f_7^{1,+} + f_8^{1,+}) + \frac{1}{3}\phi_0. \quad (56)$$

Substituting Eq. (44) into Eq. (56) results in the following equation

$$f_2^1 + f_5^1 + f_6^1 = -\left[\frac{2-k_1}{6}\phi_1 + (k_1-1)(f_2^1 + f_5^1 + f_6^1) + \frac{1}{6}\Delta tS - \left(1 - \frac{k_1}{2} - \frac{k_2}{2}\right)\frac{2}{3k_2}\Delta tS\right] + \frac{1}{3}\phi_0, \quad (57)$$

If we substitute Eq. (57) into Eq. (42), one can obtain

$$k_1(f_4^1 + f_7^1 + f_8^1) = \frac{2+k_1}{6}\phi_1 - \frac{1}{3}\phi_0 - \frac{2k_1}{3k_2}\Delta tS + \frac{1}{6}\Delta tS - \left(1 - \frac{k_1}{2} - \frac{k_2}{2}\right)\frac{2}{3k_2}\Delta tS, \quad (58)$$

then substituting Eq. (52) into Eq. (58) yields

$$3\phi_1 - \phi_2 - 2\phi_0 = \frac{4k_1}{k_2}\Delta tS + \frac{12(k_1-1)}{2-k_1}\left[\frac{1}{6}\Delta tS - \left(1 - \frac{k_1}{2} - \frac{k_2}{2}\right)\frac{2}{3k_2}\Delta tS\right]. \quad (59)$$

Finally, the *numerical slip* can be obtain through substituting Eq. (49), Eq. (50) into Eq. (59),

$$\phi_s = \frac{3k_1k_2 - 8k_1 - 12k_2 + 16}{12k_1k_2} \frac{\Delta\phi}{N^2}. \quad (60)$$

Let $\phi_s = 0$, we can obtain the following expression,

$$k_2 = \frac{8(k_1-2)}{3(k_1-4)}, \quad (61)$$

which can be used to eliminate the *numerical slip*.

4. Numerical results and discussion

To test the stability and accuracy of present model, some simulations of isotropic CDEs and anisotropic CDEs are performed. The HBB scheme [77] is adopted to treat the Dirichlet boundary conditions. In our simulations, the following global relative error (GRE) is used to measure the accuracy of the present B-TriRT model,

$$GRE = \frac{\sum_{i,j} |\phi(\mathbf{x}, t) - \phi^*(\mathbf{x}, t)|}{\sum_{i,j} |\phi^*(\mathbf{x}, t)|}, \quad (62)$$

where ϕ and ϕ^* are the numerical and analytical solution, respectively. Besides, for the steady flows, the following convergent criterion is adopted,

$$\frac{\sum_{i,j} |\phi(\mathbf{x}, t + 1000\Delta t) - \phi(\mathbf{x}, t)|}{\sum_{i,j} |\phi(\mathbf{x}, t + 1000\Delta t)|} < 10^{-10}. \quad (63)$$

Unless otherwise stated, the distribution function $f_i(\mathbf{x}, t)$ is initialized by its equilibrium distribution function $f_i^{eq}(\mathbf{x}, t)$, and the tunable parameter Z in MLBM is set as 0.0001 for a satisfactory accuracy.

4.1. Isotropic CDEs

4.1.1. A steady diffusion problem

In this part, we will validate the expression [Eq. (61)] by conducting some simulations of a steady diffusion problem in the physical region $[0, L] \times [0, L]$, which can be described by Eqs. (33)-(34).

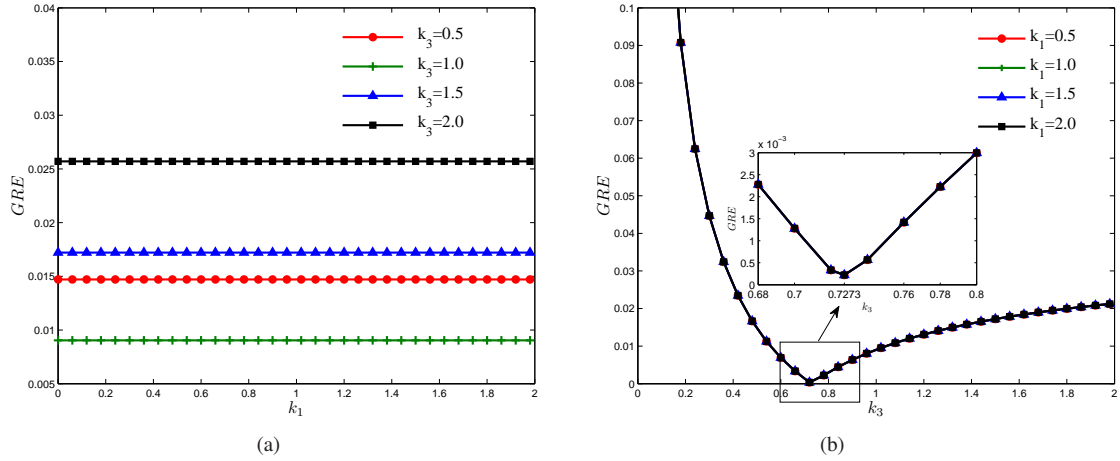


Figure 2: The global relative errors at different relaxation parameters [(a): the effects of k_0 (b): the effects of k_2].

For isotropic CDEs, the relaxation parameters could be simplified as $\mathbf{K}_1 = k_1 \mathbf{I}$, $\mathbf{K}_2 = k_2 \hat{\mathbf{I}}$. In the simulations, $L = 1.0$, $u_x = 0.1$, $\alpha = 0.1$, $\phi_L = 1.0$, $\phi_0 = 0$, $\Delta x = L/5$, $k_1 = 1.25$. We first investigated the effects of tunable relaxation parameters k_0 and k_2 on the accuracy of present B-TriRT model, and presented the results in Fig. 2. From

Fig. 2(a), one can observe that the relaxation parameter k_0 has no distinct effect on the accuracy of present model. The reason is simple: from the matrix analysis, one can find that the parameter k_0 is related to the zero-order moment of non-equilibrium distribution function f_i^{neq} , and has no influence on the derivation of Eq. (47). On the other hand, the relaxation parameter k_2 plays an important role in the accuracy of present model. From the inserted figure in Fig. 2(b), the optimal k_2 for this specific simulation is 0.7273, which is consistent with the relational expression $k_2 = [8(k_1 - 2)]/[3(k_1 - 4)] = 0.7273$.

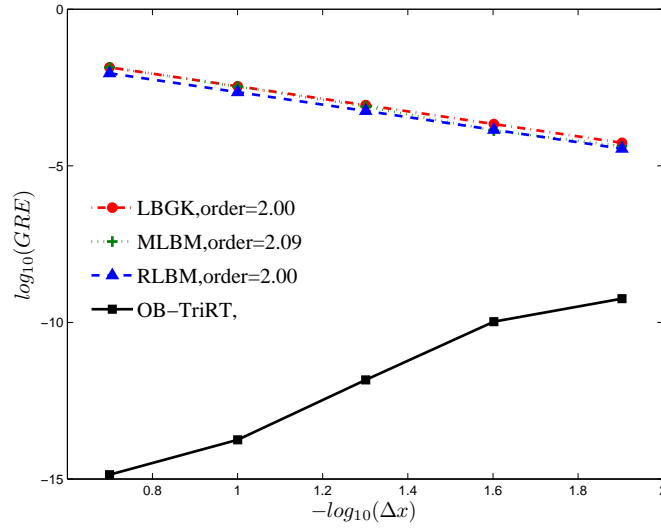


Figure 3: The global relative errors of different models at different mesh sizes.

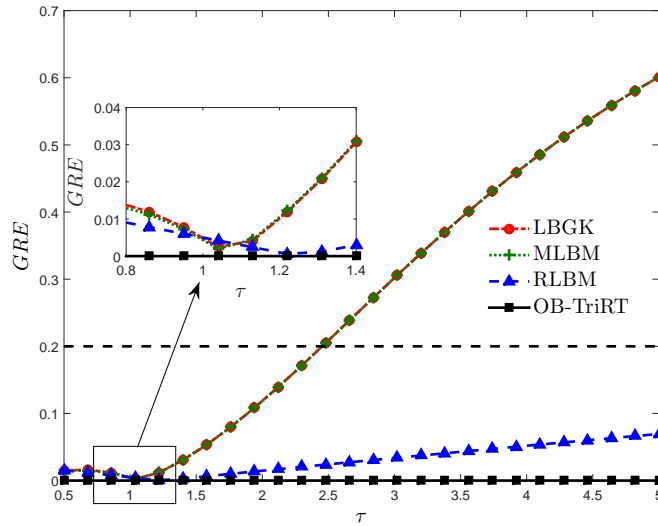


Figure 4: The global relative of different models errors at different relaxation times.

Furthermore, to test the convergence rate of present model, we also perform some simulation with different mesh

Table 2: The comparison of numerical efficiency among different models

Model	Mesh: $\Delta x = 1/5$		Mesh: $\Delta x = 1/10$	
	Time of 100 steps (s)	Time of steady state (s)	Time of 100 steps (s)	Time of steady state (s)
LBGK	0.005	0.022	0.017	0.276
MLBM	0.020	0.088	0.062	1.214
RLBM	0.020	0.088	0.062	1.201
MRT	0.051	0.264	0.162	3.010
OB-TriRT	0.039	0.231	0.149	2.786

resolutions ($\Delta x = L/5, L/10, L/20, L/40, L/80$), and presented the *GREs* in Fig. 3, where the optimal block triple-relaxation-time (OB-TriRT) lattice Boltzmann model corresponds to the case with $k_0 = 1, k_1 = 1/\tau, k_2 = [8(k_1 - 2)]/[3(k_1 - 4)]$. As shown in Fig. 3, both LBGK, MLBM and RLBM have a second-order accuracy in space, while the magnitude of *GREs* in OB-TriRT model is around 10^{-10} , which is close to the machine Error. Actually, the *GREs* of OB-TriRT model could be zero since the *numerical slip* is completely eliminated, and the present *GREs* are caused by the machine error.

Then, we carried out some simulations under different value of relaxation time τ to investigate the stability of different models. From Fig. 4, one can clearly find that the OB-TriRT model is more stable than other models. Besides, the RLBM is more stable than LBGK and MLBM, the result is consistent with the previous work [61]. Moreover, the results in Fig. 4 also indicate that the *numerical slip* is completely eliminated by the adoption of expression $k_2 = [8(k_1 - 2)]/[3(k_1 - 4)]$.

Finally, we conducted a simple test on an Intel Core i5-8250U CPU and gave a comparison in the Tab. 2. From the table, one can obtain that the present model doesn't show the best numerical efficiency due to the calculation of first-order and second-order moments of the non-equilibrium distribution. However, the present model has better numerical efficiency than the MRT model.

4.1.2. Convection-diffusion equation with a constant velocity

Now, we consider the following linear isotropic convection-diffusion equation,

$$\partial_t \phi + \nabla \cdot (\phi \mathbf{u}) = \nabla \cdot (\alpha \nabla \phi) + S, \quad (64)$$

where $\mathbf{u} = (u_x, u_y)^T$ is a constant velocity, α is the diffusion coefficient. S is the source term, which is given by $S = \exp[(1 - 2\pi^2\alpha)t] \sin[\pi(x + y)] + \pi(u_x + u_y) \cos[\pi(x + y)]$. Under the proper initial and boundary conditions, the analytical solution of this problem can be given as

$$\phi(x, y, t) = \exp[(1 - 2\pi\alpha)t] \sin[\pi(x + y)]. \quad (65)$$

In the simulations, the computational domain is fixed to be $[0, 2] \times [0, 2]$. We first performed some simulations under different time and different diffusion coefficients, and presented the results in Fig. 5 where $c = 1.0$, $u_x = u_y = 0.1$, the mesh size is 200×200 . As we can see from the figure, the numerical solutions agree well with analytical solutions, even with a small diffusion coefficient. The *GREs* at time $t = 3$ are 3.009×10^{-3} for $\alpha = 0.01$ and 1.745×10^{-4} for $\alpha = 0.0001$.

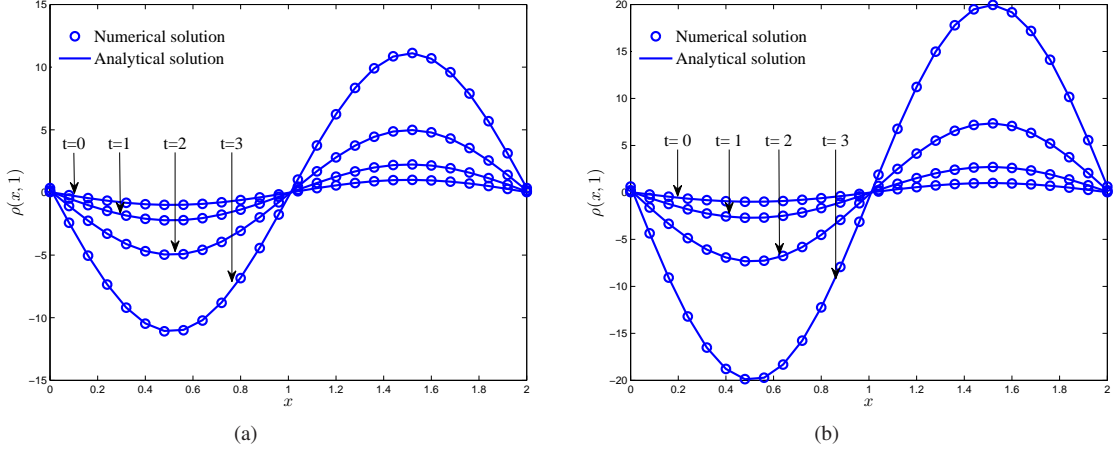


Figure 5: Numerical and analytical solutions at different time and diffusion coefficients [(a): $\alpha = 0.01$ (b): $\alpha = 0.0001$].

We also tested the convergence rate of present model, and conducted a number of simulations under different mesh resolutions $\Delta x = 1/25, 1/50, 1/100, 1/200$ with τ being fixed at 0.8. The results shown in Fig. 6 indicate that all the LBGK, MLBM, RLBM and OB-TriRT model have a second-order accuracy in space, and the OB-TriRT model is more accurate than other models. In addition, the *GREs* of OB-TriRT model are different from the results in Fig. 3, it means that the *numerical slip* hasn't been completely eliminated. However, the adoption of expression $[k3 = 8(k_1 - 2)]/[3(k_1 - 4)]$ can still bring some benefits in accuracy.

Furthermore, to investigate the stability of present OB-TriRT model for the problem with different convection velocity ($u_0 = 0.01, 0.1, 1.0, 2.5$), we carried out some simulations with $\Delta x = 1/50$, $c = 5.0$, $\tau = 0.8$, $\alpha = 0.01$, $t = 1$, $u_x = u_y = u_0$, and presented a quantitative comparison in Tab. 3. As shown in this table, all models are unstable for the case $u_0 = 2.5$ except for the OB-TriRT model, which indicates that the present OB-TriRT model is more accurate than other models. Accordingly, the results also indicate that the expression $[k3 = 8(k_1 - 2)]/[3(k_1 - 4)]$ could be used to improve the stability of present model.

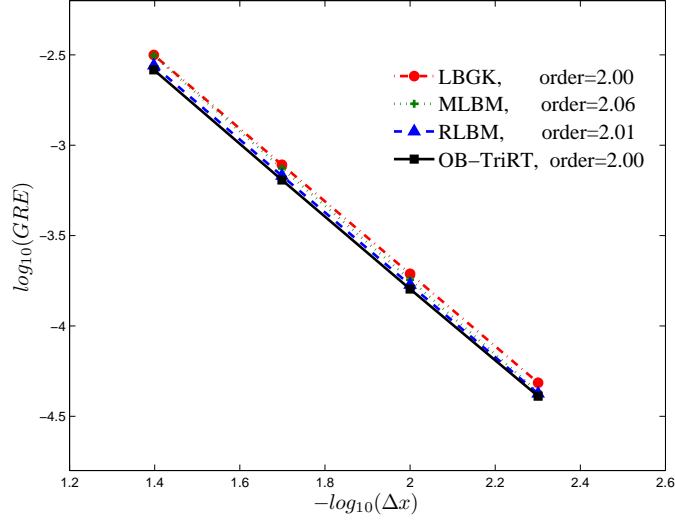


Figure 6: The global relative errors of different models at different mesh sizes.

Table 3: The global relative errors of different models at different convection velocities ("-" :unstable)

Model	$u_0 = 0.01$	$u_0 = 0.1$	$u_0 = 1.0$	$u_0 = 2.5$
LBGK	7.5225×10^{-4}	7.7943×10^{-4}	2.6979×10^{-3}	-
MLBM	3.9366×10^{-4}	4.5053×10^{-4}	2.6503×10^{-3}	-
RLBM	6.9176×10^{-4}	6.7784×10^{-4}	3.4796×10^{-3}	-
OB-TriRT	5.8108×10^{-4}	6.5226×10^{-4}	2.1399×10^{-3}	1.7531×10^{-2}

4.1.3. Burgers-Fisher equation

The Burgers-Fisher equation (BFE), as a special case of the nonlinear CDE and a popular benchmark problem, is also adopted to test the present OB-TriRT model. The BFE can be expressed as [79]

$$\partial_t \phi + a\phi^\delta \partial_x \phi = \alpha(\partial_{xx} \phi + \partial_{yy} \phi) + b\phi(1 - \phi^\delta), \quad (66)$$

where δ , b are constants, a, α are the constant convection and diffusion coefficients. Under the proper initial and boundary conditions, the analytical solution can be expressed as

$$\phi(x, y, t) = \left\{ \frac{1}{2} + \frac{1}{2} \tanh[A(x + y - \omega t)] \right\}^{\frac{1}{\delta}}, \quad (67)$$

where A and ω are defined as

$$A = -\frac{a\delta}{4\alpha(\delta + 1)}, \quad \omega = \frac{a^2 + 2b\alpha(\delta + 1)}{a(\delta + 1)}. \quad (68)$$

The simulations are performed on domain $[-1, 2] \times [-1, 2]$, and the effect of coefficients a and α are mainly investigated for different models. Firstly, we tested the capacity of present OB-TriRT model in solving the nonlinear

BFE, and presented the numerical and analytical solutions at different time and different diffusion coefficients in Fig. 7 where $\Delta x = 1/160$, $c = 5$, $a = 2.0$, $b = 0.05$, $\delta = 1.5$. As shown in the figure, the numerical solutions are in good agreement with analytical solutions. We also calculated the difference between the analytical solutions and numerical solutions at time $t = 2.0$, and found that $GREs = 4.7266 \times 10^{-5}$, 1.1247×10^{-4} for $\alpha = 0.05, 0.005$ respectively. The results show that the present OB-TriRT model has the ability in solving nonlinear CDEs, even with a small diffusion coefficient.

Then, we tested the convergence rate of present OB-TriRT model by conducting a number of simulations under different mesh resolutions ($\Delta x = 1/20, 1/40, 1/80, 1/160$) with $a = 2.0$, $b = 0.05$, $\delta = 1.5$, $\alpha = 0.01, t = 1.0$. The results shown in Fig. 8 indicate that present OB-TriRT model has a second-order convergence rate in space. In addition, the $GREs$ of OB-TriRT model are smaller than other models, which implies that the expression $[k_3 = 8(k_1 - 2)]/[3(k_1 - 4)]$ can be used to improve the accuracy of present model.

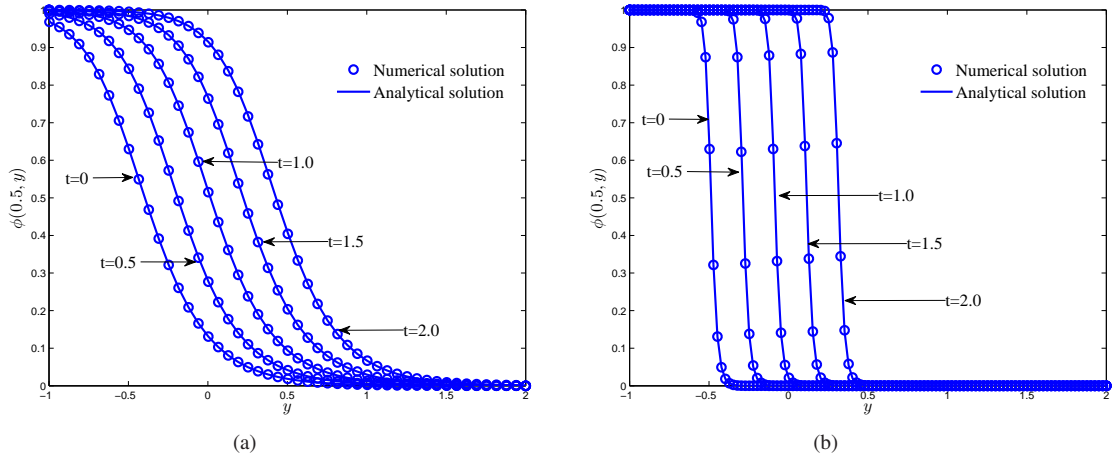


Figure 7: Numerical and analytical solutions at different time and diffusion coefficients [(a): $\alpha = 0.05$ (b): $\alpha = 0.0005$].

Table 4: The global relative errors of different models at different convection coefficients with $\alpha = 0.05$ ("-" :unstable)

Model	$a = 1$	$a = 2$	$a = 3$	$a = 4$
LBGK	1.1958×10^{-3}	3.2058×10^{-3}	4.1915×10^{-3}	-
MLBM	1.2038×10^{-3}	3.2015×10^{-3}	1.1927×10^{-3}	-
RLBM	5.2339×10^{-4}	9.9594×10^{-4}	1.1328×10^{-3}	-
OB-TriRT	5.0193×10^{-4}	9.5559×10^{-4}	1.0653×10^{-3}	2.2140×10^{-3}

Finally, we turn to investigate the effects of coefficients a and α , and present a comparison of different models in Tab. 4 and Tab. 5 where $\Delta x = 1/40$, $c = 5$, $b = 0.05$, $\delta = 1.5$. As shown in Tab. 4, when a increases from 1 to 4, the $GREs$ increase. In addition, when a is increased to 4, all models are unstable apart from OB-TriRT model. Moreover, the results show that the OB-TriRT model could be more accurate than other models under the present parameters.

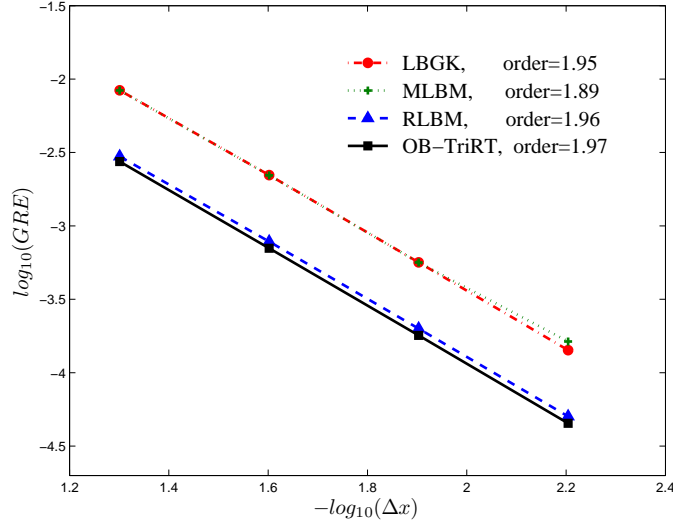


Figure 8: The global relative errors of different models at different mesh sizes.

Table 5: The global relative errors of different models at different convection coefficients with $a = 2$ ("-" :unstable)

Model	$\alpha = 0.005$	$\alpha = 0.05$	$\alpha = 0.1$	$\alpha = 0.5$
LBGK	-	3.2058×10^{-3}	5.7829×10^{-3}	-
MLBM	-	3.2015×10^{-4}	5.7852×10^{-3}	-
RLBM	4.7209×10^{-3}	9.9594×10^{-4}	1.8174×10^{-3}	1.7866×10^{-3}
OB-TriRT	9.6078×10^{-3}	9.5559×10^{-4}	2.0497×10^{-3}	2.0271×10^{-3}

From Tab. 5, one can obtain that the LBGK and MLBM are unstable at $\alpha = 0.005$ and $\alpha = 0.5$. Moreover, under the present parameters, the *GREs* of OB-TriRT model are not always less than RLBM, that implies the expression $k_2 = [8(k_1 - 2)]/[3(k_1 - 4)]$ may be not the optimal choice for some nonlinear CDEs. However, as discussed above, the adoption of this expression still could give a satisfactory results for the complicated nonlinear problems.

4.2. Anisotropic CDEs

4.2.1. Gaussian hill problem

In the following parts, we turn to test the capacity of present B-TriRT model in solving anisotropic CDEs. On the one hand, the anisotropic problems could not be solved directly by the previous LBGK model [38] due to the diffusion coefficient is not a scalar variable. On the other hand, although the MRT model has the ability in the study of the anisotropic problems, it is not convenient to determine the free relaxation parameters, and the additional multiple-relaxation collision will reduce the computational efficiency. It should be mentioned that, for anisotropic CDEs, the parameter related to diffusion coefficient is a matrix \mathbf{K}_1 rather than a constant k_1 , which can be determined by Eq. (32). Moreover, the expression Eq. (61) between k_1 and k_2 no longer exists. Without loss of generality, the parameter k_2 is set to be 1 for all simulations of the anisotropic CDEs. Firstly, we consider a classic benchmark example named

Gaussian hill, which can be described by

$$\partial_t \phi + \nabla \cdot (\phi \mathbf{u}) = \nabla \cdot (\mathbf{A} \cdot \nabla \phi), \quad (69)$$

where $\mathbf{u} = (u_x, u_y)^T$ is a constant velocity, \mathbf{A} is a constant diffusion tensor. The analytical solution to this problem can be given by

$$\phi(\mathbf{x}, t) = \frac{\phi_0}{2\pi \sqrt{|\det(\sigma_t)|}} \exp \left\{ -\frac{1}{2} \sigma_t^{-1} : [(\mathbf{x} - \mathbf{u}t)(\mathbf{x} - \mathbf{u}t)] \right\}, \quad (70)$$

where $\sigma_t = \sigma_0^2 \mathbf{I} + 2\mathbf{A}t$, $|\det(\sigma_t)|$ is absolute value of the determinant of σ_t , σ_t^{-1} is the inverse matrix of σ_t . In our simulations, the computational domain is fixed on $[-1, 1] \times [-1, 1]$, $\sigma_0 = 0.01$, $u_x = u_y = 0.01$, and the following diffusion matrices are considered,

$$\mathbf{A} = \left[\left[\begin{array}{cc} 1 & 0 \\ 0 & 1 \end{array} \right], \left[\begin{array}{cc} 1 & 0 \\ 0 & 2 \end{array} \right], \left[\begin{array}{cc} 1 & 1 \\ 1 & 2 \end{array} \right] \right] \times 10^{-3}, \quad (71)$$

which are usually denoted as isotropic, diagonally anisotropic and fully anisotropic diffusion problems [49].

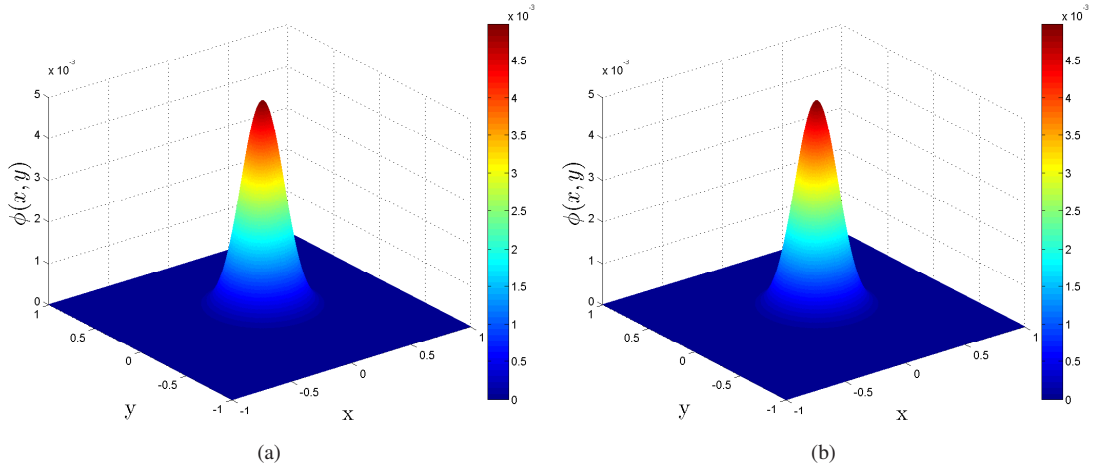


Figure 9: Numerical and analytical solutions at $t = 10$ [(a): numerical solution (b): analytical solution].

A number of simulations are conducted to test the capacity of present model B-TriRT model for the anisotropic CDEs, and the results at time $t = 10$ are presented in Figs. 9-11 where $\Delta x = 1/400$, $c = 1.0$. As seen from these figures, one can find that the numerical solutions qualitatively agree well with analytical solutions. To give a quantitative comparison, we also calculated the *GREs* of three types of anisotropic diffusion problem at time $t = 10$, and the values of *GREs* are 4.5926×10^{-5} , 6.0109×10^{-5} and 1.3145×10^{-4} , respectively. These results indicate that the present B-TriRT model can solve anisotropic CDEs accurately. Furthermore, we tested the convergence rate of

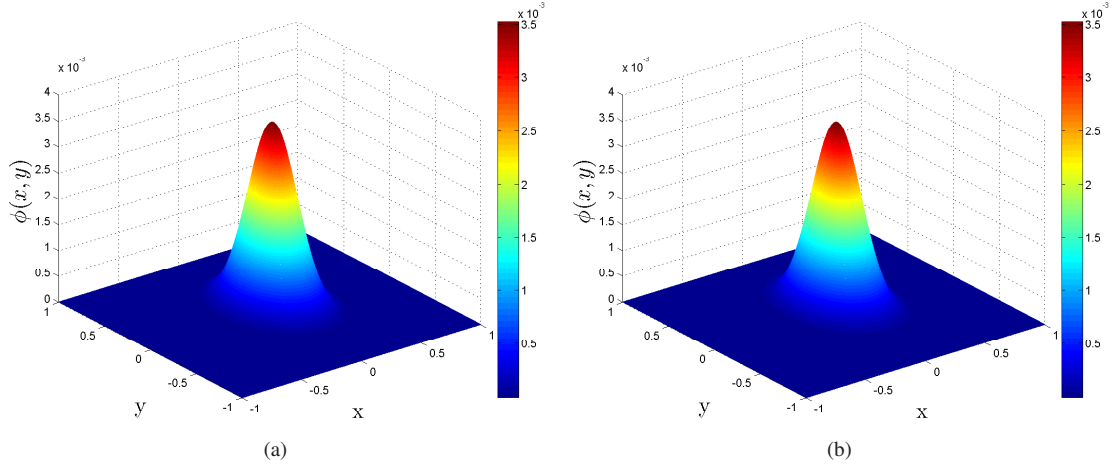


Figure 10: Numerical and analytical solutions at $t = 10$ [(a): numerical solution (b): analytical solution].

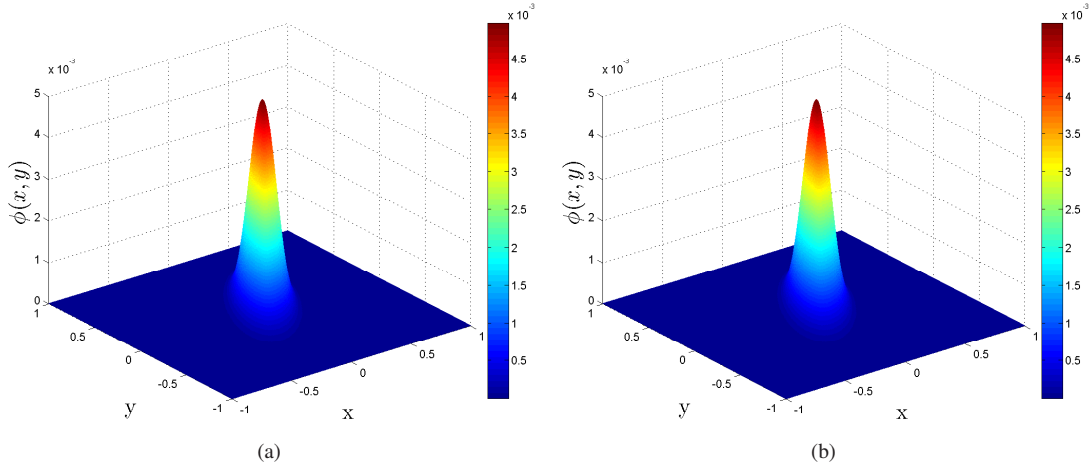


Figure 11: Numerical and analytical solutions at $t = 10$ [(a): numerical solution (b): analytical solution].

present B-TriRT model by carrying out some simulations with $\Delta x^2/\Delta t = 5.0 \times 10^{-3}$ under different mesh resolutions ($\Delta x = 1/100, 1/200, 1/400, 1/800$), and the relationship between GRE and lattice spacing Δx is illustrated in Fig. 12. From this figure, one can obtain that the present B-TriRT model has a second-order accuracy in space for all types of anisotropic diffusion problems.

4.2.2. Anisotropic convection-diffusion equation with variable diffusion tensor

Actually, the LBGK model can also be used to solve the above Gaussian hill problem by rewriting the macroscopic equation (69) into an isotropic form. For a more complicated problem with variable diffusion tensor, however, it is difficult or impossible to write it into an isotropic form. Here we consider the following problem depicted by [49],

$$\partial_t \phi + \nabla \cdot (\phi \mathbf{u}) = \nabla \cdot (\mathbf{A} \cdot \nabla \phi) + S, \quad (72)$$

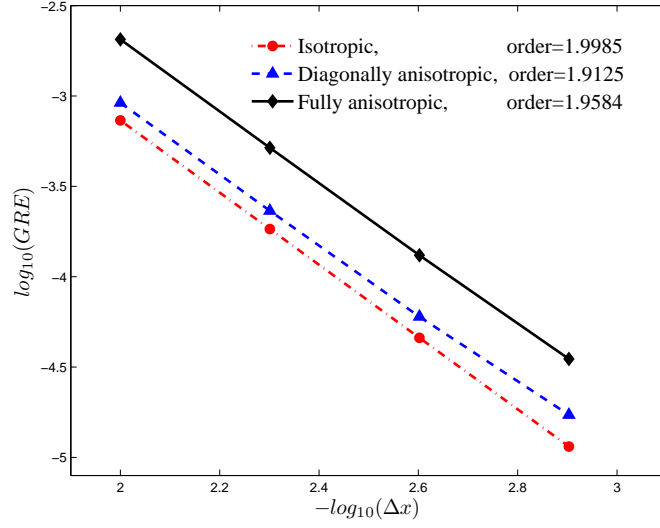


Figure 12: The global relative errors of different problems at different mesh sizes.

where $\mathbf{u} = (u_x, u_y)^T$ is a constant velocity, $\mathbf{A}(\mathbf{x}, \phi)$ is a function of space $\mathbf{x} = (x, y)$ and scalar variable ϕ , and S is the source term.

In our simulations, the variable diffusion tensor \mathbf{A} is given by

$$\mathbf{A} = \begin{pmatrix} 2 - \sin(2\pi x)\sin(2\pi y) & 0 \\ 0 & 1 \end{pmatrix} \alpha, \quad (73)$$

where α is a constant. The analytical solution of this problem is given as

$$\phi(x, y, t) = \exp[(1 - 12\pi^2\alpha)t]\sin(2\pi x)\sin(2\pi y), \quad (74)$$

the source term S can be expressed as

$$S = \exp[(1 - 12\pi^2\alpha)t]\{\sin(2\pi x)\sin(2\pi y) + 4\alpha\pi^2\cos(4\pi x)\sin^2(2\pi y) + 2\pi[u_x\cos(2\pi x)\sin(2\pi y) + u_y\sin(2\pi x)\cos(2\pi y)]\}. \quad (75)$$

We conducted some simulations with $u_x = u_y = 0.1$, $\alpha = 1.0 \times 10^{-2}$, $\Delta x = 1/400$, $c = 1.0$ under different time ($t = 3$, $t = 10$), and presented the numerical and analytical results in Figs. 13-14. And the corresponding $GREs$ are 4.7266×10^{-5} and 4.4733×10^{-5} . All the results indicate that the present B-TriRT model is accurate in solving the anisotropic CDEs with a variable diffusion tensor. In addition, we also investigated the effects of α under different mesh resolutions ($\Delta x = 1/50$, $1/100$, $1/200$, $1/400$), and presented the results in Tab. 6. From the table, one can obtain that the present B-TriRT model is also accurate even for the case with a much smaller α . Based on Tab. 6, we

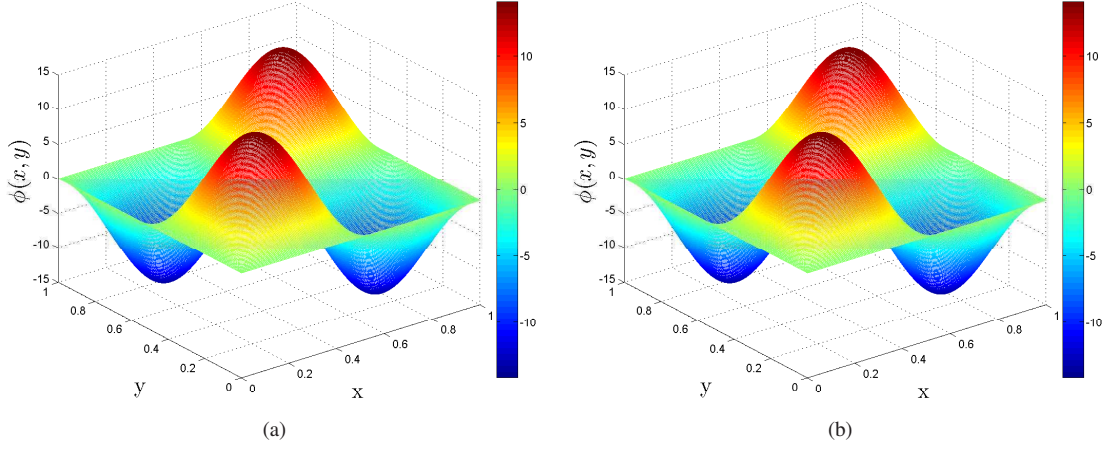


Figure 13: Numerical and analytical solutions at $t = 3$ [(a): numerical solution (b): analytical solution].

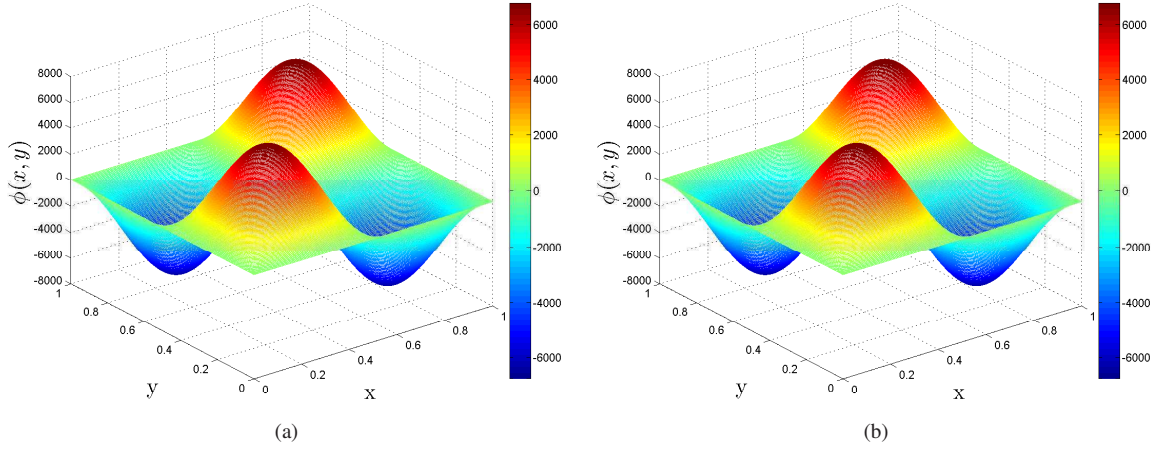


Figure 14: Numerical and analytical solutions at $t = 10$ [(a): numerical solution (b): analytical solution].

also computed the convergence rate of B-TriRT model, and the results are shown in Fig. 15. As seen from the figure, the present B-TriRT model also has a second-order convergence rate in space for this complicated anisotropic CDEs.

5. Conclusions

In this work, we presented a block triple-relaxation-time lattice Boltzmann model for general nonlinear anisotropic convection-diffusion equations, where RLBM and MLBM are its special cases. Furthermore, we expand the non-equilibrium distribution function to the second-order moment by Hermite polynomial to obtain the present B-TriRT model. In addition, the present B-TriRT model also has some striking features, which are summarized as follows:

1. The Chapman-Enskog analysis of present B-TriRT model is simple since it can be conducted under the LBGK framework.

Table 6: The global relative errors of different α under different mesh resolutions

α	$\Delta x = 1/50$	$\Delta x = 1/100$	$\Delta x = 1/200$	$\Delta x = 1/400$
1.0×10^{-2}	2.8801×10^{-3}	7.2875×10^{-4}	1.8768×10^{-4}	4.7266×10^{-5}
1.0×10^{-4}	5.1174×10^{-3}	8.2137×10^{-4}	1.7601×10^{-4}	4.2156×10^{-5}
1.0×10^{-6}	5.2599×10^{-3}	9.2122×10^{-4}	1.7660×10^{-4}	4.1732×10^{-5}

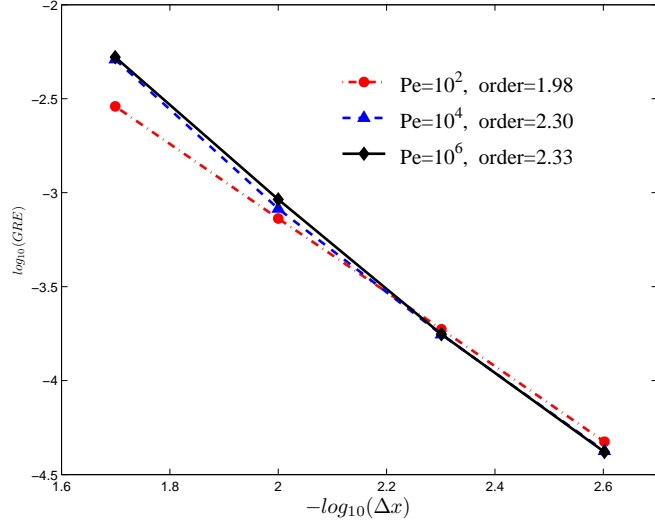


Figure 15: The global relative errors of different Pe at different mesh sizes.

2. Based on the matrix analysis, we partitioned the relaxation parameter matrix \mathbf{S}_f into three relaxation parameter blocks, i.e., \mathbf{S}_0 , \mathbf{S}_1 , \mathbf{S}_2 , which correspond to the remaining, first-order and second-order moments of non-equilibrium distribution function, respectively.
3. Based on the analysis of HBB scheme for Dirichlet boundary conditions, we obtained an expression to determine the relation between relaxation parameters.
4. The anisotropic diffusion tensor can be recovered ingeniously by relaxation parameter matrix \mathbf{K}_1 .

Finally, several numerical simulations (including isotropic and anisotropic CDEs) are performed, and the results show that the present model has a second-order accuracy in space, and is usually more accurate and stable than some available lattice Boltzmann models. In addition, the present B-TriRT LBM can be extended to solve the NSEs where the viscosity is related to the relaxation matrix \mathbf{K}_2 , which would be considered in a future work.

6. Acknowledgments

This work is supported by the National Natural Science Foundation of China (Grants No. 51576079 and No. 51836003), and the National Key Research and Development Program of China (Grant No. 2017YFE0100100).

7. Appendixs

7.1. A matrix analysis

In this part, we will partition the relaxation parameter matrix into three relaxation parameter blocks. Now, we first rewrite the evolution Eq. (5) in a vector form:

$$\mathbf{f}^\dagger = \mathbf{f} - k_0 \mathbf{f}^{neq} - \mathbf{R} \mathbf{f}^{neq} - \mathbf{P} \mathbf{f}^{neq} + \Delta t \mathbf{G} + \Delta t S + \frac{\Delta t^2}{2} \bar{D} S, \quad (76)$$

where $\mathbf{f} = [f_0(\mathbf{x}, t), f_1(\mathbf{x}, t), f_2(\mathbf{x}, t), \dots, f_{q-1}(\mathbf{x}, t)]^T$. The matrices \mathbf{R} and \mathbf{P} are given by

$$\mathbf{R}_{ij} = \frac{\omega_i \mathbf{c}_i \cdot [(\mathbf{K}_1 - k_0 \mathbf{I}) \mathbf{c}_j]}{c_s^2}, \quad \mathbf{P}_{ij} = \frac{\omega_i (\mathbf{c}_i \mathbf{c}_i - c_s^2 \mathbf{I}) : [(\mathbf{K}_2 - k_0 \hat{\mathbf{I}}) \circ (\mathbf{c}_j \mathbf{c}_j)]}{2c_s^4}, \quad (77)$$

For simplicity, $\mathbf{K}_1 = k_1 \mathbf{I}$, $\mathbf{K}_2 = k_2 \hat{\mathbf{I}}$ is first considered in the following matrix analysis. Then, considering the popular D2Q9 lattice model, the explicit forms of \mathbf{R} and \mathbf{P} are given by

$$\mathbf{R} = \frac{k_1 - k_0}{12} \begin{pmatrix} 0 & 0 & 0 & 0 & 0 & 0 & 0 & 0 & 0 \\ 0 & 4 & 0 & -4 & 0 & 4 & -4 & -4 & 4 \\ 0 & 0 & 4 & 0 & -4 & 4 & 4 & -4 & -4 \\ 0 & -4 & 0 & 4 & 0 & -4 & 4 & 4 & -4 \\ 0 & 0 & -4 & 0 & 4 & -4 & -4 & 4 & 4 \\ 0 & 1 & 1 & -1 & -1 & 2 & 0 & -2 & 0 \\ 0 & -1 & 1 & 1 & -1 & 0 & 2 & 0 & -2 \\ 0 & -1 & -1 & 1 & 1 & -2 & 0 & 2 & 0 \\ 0 & 1 & -1 & -1 & 1 & 0 & -2 & 0 & 2 \end{pmatrix}, \quad (78)$$

$$\mathbf{P} = \frac{k_2 - k_0}{12} \begin{pmatrix} 0 & -8 & -8 & -8 & -8 & -16 & -16 & -16 & -16 \\ 0 & 4 & -2 & 4 & -2 & 2 & 2 & 2 & 2 \\ 0 & -2 & 4 & -2 & 4 & 2 & 2 & 2 & 2 \\ 0 & 4 & -2 & 4 & -2 & 2 & 2 & 2 & 2 \\ 0 & -2 & 4 & -2 & 4 & 2 & 2 & 2 & 2 \\ 0 & 1 & 1 & 1 & 1 & 5 & -1 & 5 & -1 \\ 0 & 1 & 1 & 1 & 1 & -1 & 5 & -1 & 5 \\ 0 & 1 & 1 & 1 & 1 & 5 & -1 & 5 & -1 \\ 0 & 1 & 1 & 1 & 1 & -1 & 5 & -1 & 5 \end{pmatrix}. \quad (79)$$

However, for the D3Q19 lattice model, the matrices \mathbf{R}, \mathbf{P} can be written as

$$\mathbf{R} = \frac{k_1 - k_0}{12} \begin{pmatrix} 0 & 0 & 0 & 0 & 0 & 0 & 0 & 0 & 0 & 0 & 0 & 0 & 0 & 0 & 0 & 0 & 0 & 0 \\ 0 & 2 & -2 & 0 & 0 & 0 & 0 & 2 & -2 & 2 & -2 & 2 & -2 & 2 & -2 & 0 & 0 & 0 \\ 0 & -2 & 2 & 0 & 0 & 0 & 0 & 2 & 2 & -2 & 2 & -2 & 2 & -2 & 2 & 0 & 0 & 0 \\ 0 & 0 & 0 & 2 & -2 & 0 & 0 & 2 & 2 & -2 & -2 & 0 & 0 & 0 & 0 & 2 & -2 & 2 \\ 0 & 0 & 0 & -2 & 2 & 0 & 0 & -2 & -2 & 2 & 2 & 0 & 0 & 0 & 0 & -2 & 2 & -2 \\ 0 & 0 & 0 & 0 & 0 & 2 & -2 & 0 & 0 & 0 & 0 & 2 & 2 & -2 & -2 & 2 & 2 & -2 \\ 0 & 0 & 0 & 0 & 0 & -2 & 2 & 0 & 0 & 0 & 0 & -2 & -2 & 2 & 2 & -2 & -2 & 2 \\ 0 & 1 & -1 & 1 & -1 & 0 & 0 & 2 & 0 & 0 & -2 & 1 & -1 & 1 & -1 & 1 & -1 & 1 \\ 0 & -1 & 1 & 1 & -1 & 0 & 0 & 0 & 2 & -2 & 0 & -1 & 1 & -1 & 1 & 1 & -1 & 1 \\ 0 & 1 & -1 & -1 & 1 & 0 & 0 & 0 & -2 & 2 & 0 & 1 & -1 & 1 & -1 & -1 & 1 & -1 \\ 0 & -1 & 1 & -1 & 1 & 0 & 0 & -2 & 0 & 0 & 2 & -1 & 1 & -1 & 1 & -1 & 1 & -1 \\ 0 & 1 & -1 & 0 & 0 & 1 & -1 & 1 & -1 & 1 & -1 & 2 & 0 & 0 & -2 & 1 & 1 & -1 \\ 0 & -1 & 1 & 0 & 0 & 1 & -1 & -1 & 1 & -1 & 1 & 0 & 2 & -2 & 0 & 1 & 1 & -1 \\ 0 & 1 & -1 & 0 & 0 & -1 & 1 & 1 & -1 & 1 & -1 & 0 & -2 & 2 & 0 & -1 & -1 & 1 \\ 0 & -1 & 1 & 0 & 0 & -1 & 1 & -1 & 1 & -1 & 1 & -2 & 0 & 0 & 2 & -1 & -1 & 1 \\ 0 & 0 & 0 & 1 & -1 & 1 & -1 & 1 & 1 & -1 & -1 & 1 & 1 & -1 & -1 & 2 & 0 & 0 \\ 0 & 0 & 0 & -1 & 1 & 1 & -1 & -1 & -1 & 1 & 1 & 1 & 1 & -1 & -1 & 0 & 2 & -2 \\ 0 & 0 & 0 & 1 & -1 & -1 & 1 & 1 & 1 & -1 & -1 & -1 & -1 & 1 & 1 & 0 & -2 & 2 \\ 0 & 0 & 0 & -1 & 1 & -1 & 1 & -1 & -1 & 1 & 1 & -1 & -1 & 1 & 1 & -2 & 0 & 2 \end{pmatrix}, \quad (80)$$

$$\mathbf{P} = \frac{k_2 - k_0}{24} \begin{pmatrix}
0 & -12 & -12 & -12 & -12 & -12 & -12 & -24 & -24 & -24 & -24 & -24 & -24 & -24 & -24 & -24 & -24 & -24 & -24 \\
0 & 4 & 4 & -2 & -2 & -2 & -2 & 2 & 2 & 2 & 2 & 2 & 2 & 2 & 2 & -4 & -4 & -4 & -4 \\
0 & 4 & 4 & -2 & -2 & -2 & -2 & 2 & 2 & 2 & 2 & 2 & 2 & 2 & 2 & -4 & -4 & -4 & -4 \\
0 & -2 & -2 & 4 & 4 & -2 & -2 & 2 & 2 & 2 & 2 & -4 & -4 & -4 & -4 & 2 & 2 & 2 & 2 \\
0 & -2 & -2 & 4 & 4 & -2 & -2 & 2 & 2 & 2 & 2 & -4 & -4 & -4 & -4 & 2 & 2 & 2 & 2 \\
0 & -2 & -2 & -2 & -2 & 4 & 4 & -4 & -4 & -4 & -4 & 2 & 2 & 2 & 2 & 2 & 2 & 2 & 2 \\
0 & -2 & -2 & -2 & -2 & 4 & 4 & -4 & -4 & -4 & -4 & 2 & 2 & 2 & 2 & 2 & 2 & 2 & 2 \\
0 & 2 & 2 & 2 & 2 & -1 & -1 & 10 & -2 & -2 & 10 & 1 & 1 & 1 & 1 & 1 & 1 & 1 & 1 \\
0 & 2 & 2 & 2 & 2 & -1 & -1 & -2 & 10 & 10 & -2 & 1 & 1 & 1 & 1 & 1 & 1 & 1 & 1 \\
0 & 2 & 2 & 2 & 2 & -1 & -1 & -2 & 10 & 10 & -2 & 1 & 1 & 1 & 1 & 1 & 1 & 1 & 1 \\
0 & 2 & 2 & 2 & 2 & -1 & -1 & 10 & -2 & -2 & 10 & 1 & 1 & 1 & 1 & 1 & 1 & 1 & 1 \\
0 & 2 & 2 & -1 & -1 & 2 & 2 & 1 & 1 & 1 & 1 & 10 & -2 & -2 & 10 & 1 & 1 & 1 & 1 \\
0 & 2 & 2 & -1 & -1 & 2 & 2 & 1 & 1 & 1 & 1 & -2 & 10 & 10 & -2 & 1 & 1 & 1 & 1 \\
0 & 2 & 2 & -1 & -1 & 2 & 2 & 1 & 1 & 1 & 1 & -2 & 10 & 10 & -2 & 1 & 1 & 1 & 1 \\
0 & 2 & 2 & -1 & -1 & 2 & 2 & 1 & 1 & 1 & 1 & 10 & -2 & -2 & 10 & 1 & 1 & 1 & 1 \\
0 & -1 & -1 & 2 & 2 & 2 & 2 & 1 & 1 & 1 & 1 & 1 & 1 & 1 & 1 & 10 & -2 & -2 & 10 \\
0 & -1 & -1 & 2 & 2 & 2 & 2 & 1 & 1 & 1 & 1 & 1 & 1 & 1 & 1 & -2 & 10 & 10 & -2 \\
0 & -1 & -1 & 2 & 2 & 2 & 2 & 1 & 1 & 1 & 1 & 1 & 1 & 1 & 1 & -2 & 10 & 10 & -2 \\
0 & -1 & -1 & 2 & 2 & 2 & 2 & 1 & 1 & 1 & 1 & 1 & 1 & 1 & 1 & 10 & -2 & -2 & 10
\end{pmatrix}.$$

(81)

As mentioned in [72], the matrices \mathbf{R} and \mathbf{P} can be diagonalized to a diagonal matrix with two and three entries of 1 respectively. In the previous works [80, 49], a transformation matrix \mathbf{M} is employed to diagonalize the collision matrices. However, we find that this matrix cannot satisfy our need for diagonalization. Following the idea in [80, 49, 72], one can determine a similar matrix \mathbf{M} . To this end, we first constructed a new invertible matrix \mathbf{C} that projects populations onto natural moments M_{opq} [81], where

$$M_{opq} = \langle f_i \mathbf{c}_{ix}^o \mathbf{c}_{iy}^p \mathbf{c}_{iz}^q \rangle, o, p, q \in \{0, 1, 2\}, \quad (82)$$

where the notation $\langle \dots \rangle$ is used as a shorthand for summation over all the velocity indices, d is the spatial dimension. From Eq. (82), one can easily obtain the transformation matrix as follows,

in the D2Q9 lattice model,

$$\mathbf{C} \cdot \mathbf{f} = (M_{000}, M_{100}, M_{010}, M_{200}, M_{110}, M_{020}, M_{210}, M_{120}, M_{220})^T, \quad (83)$$

in the D3Q19 lattice model,

$$\mathbf{C} \cdot \mathbf{f} = (M_{000}, M_{100}, M_{010}, M_{001}, M_{200}, M_{101}, M_{110}, M_{011}, M_{020}, M_{002}, M_{210}, M_{201}, M_{120}, M_{102}, M_{012}, M_{021}, M_{220}, M_{202}, M_{022})^T, \quad (84)$$

The explicit form of \mathbf{C} in D2Q9 and D3Q19 lattice models can be given as

$$\mathbf{C}_{D2Q9} = \begin{pmatrix} 1 & 1 & 1 & 1 & 1 & 1 & 1 & 1 & 1 \\ 0 & 1 & 0 & -1 & 0 & 1 & -1 & -1 & 1 \\ 0 & 0 & 1 & 0 & -1 & 1 & 1 & -1 & -1 \\ 0 & 1 & 0 & 1 & 0 & 1 & 1 & 1 & 1 \\ 0 & 0 & 0 & 0 & 0 & 1 & -1 & 1 & -1 \\ 0 & 0 & 1 & 0 & 1 & 1 & 1 & 1 & 1 \\ 0 & 0 & 0 & 0 & 0 & 1 & 1 & -1 & -1 \\ 0 & 0 & 0 & 0 & 0 & 1 & -1 & -1 & 1 \\ 0 & 0 & 0 & 0 & 0 & 1 & 1 & 1 & 1 \end{pmatrix}, \quad (85)$$

$$\mathbf{C}_{D3Q19} = \begin{pmatrix}
1 & 1 & 1 & 1 & 1 & 1 & 1 & 1 & 1 & 1 & 1 & 1 & 1 & 1 & 1 & 1 & 1 & 1 \\
0 & 1 & -1 & 0 & 0 & 0 & 0 & 1 & -1 & 1 & -1 & 1 & -1 & 1 & -1 & 0 & 0 & 0 \\
0 & 0 & 0 & 1 & -1 & 0 & 0 & 1 & 1 & -1 & -1 & 0 & 0 & 0 & 0 & 1 & -1 & 1 \\
0 & 0 & 0 & 0 & 0 & 1 & -1 & 0 & 0 & 0 & 0 & 1 & 1 & -1 & -1 & 1 & 1 & -1 \\
0 & 1 & 1 & 0 & 0 & 0 & 0 & 1 & 1 & 1 & 1 & 1 & 1 & 1 & 1 & 0 & 0 & 0 \\
0 & 0 & 0 & 0 & 0 & 0 & 0 & 0 & 0 & 0 & 0 & 1 & -1 & -1 & 1 & 0 & 0 & 0 \\
0 & 0 & 0 & 0 & 0 & 0 & 0 & 1 & -1 & -1 & 1 & 0 & 0 & 0 & 0 & 0 & 0 & 0 \\
0 & 0 & 0 & 0 & 0 & 0 & 0 & 0 & 0 & 0 & 0 & 0 & 0 & 0 & 0 & 1 & -1 & -1 \\
0 & 0 & 0 & 1 & 1 & 0 & 0 & 1 & 1 & 1 & 1 & 0 & 0 & 0 & 0 & 1 & 1 & 1 \\
0 & 0 & 0 & 0 & 0 & 1 & 1 & 0 & 0 & 0 & 0 & 1 & 1 & 1 & 1 & 1 & 1 & 1 \\
0 & 0 & 0 & 0 & 0 & 0 & 0 & 1 & 1 & -1 & -1 & 0 & 0 & 0 & 0 & 0 & 0 & 0 \\
0 & 0 & 0 & 0 & 0 & 0 & 0 & 0 & 0 & 0 & 0 & 1 & 1 & -1 & -1 & 0 & 0 & 0 \\
0 & 0 & 0 & 0 & 0 & 0 & 0 & 1 & -1 & 1 & -1 & 0 & 0 & 0 & 0 & 0 & 0 & 0 \\
0 & 0 & 0 & 0 & 0 & 0 & 0 & 0 & 0 & 0 & 0 & 1 & -1 & 1 & -1 & 0 & 0 & 0 \\
0 & 0 & 0 & 0 & 0 & 0 & 0 & 0 & 0 & 0 & 0 & 0 & 0 & 0 & 0 & 1 & -1 & 1 \\
0 & 0 & 0 & 0 & 0 & 0 & 0 & 0 & 0 & 0 & 0 & 0 & 0 & 0 & 0 & 1 & 1 & -1 \\
0 & 0 & 0 & 0 & 0 & 0 & 0 & 1 & 1 & 1 & 1 & 0 & 0 & 0 & 0 & 0 & 0 & 0 \\
0 & 0 & 0 & 0 & 0 & 0 & 0 & 0 & 0 & 0 & 0 & 1 & 1 & 1 & 1 & 0 & 0 & 0 \\
0 & 0 & 0 & 0 & 0 & 0 & 0 & 0 & 0 & 0 & 0 & 0 & 0 & 0 & 0 & 1 & 1 & 1
\end{pmatrix}. \quad (86)$$

We note that matrix \mathbf{C} cannot diagonalize the matrix \mathbf{R} or \mathbf{P} . However, through an elementary transformation

$$\mathbf{T} = \mathbf{HC} \quad (87)$$

$$\mathbf{H}_{D2Q9} = \begin{pmatrix} 1 & 0 & 0 & 0 & 0 & 0 & 0 & 0 & 0 \\ 0 & 1 & 0 & 0 & 0 & 0 & 0 & 0 & 0 \\ 0 & 0 & 1 & 0 & 0 & 0 & 0 & 0 & 0 \\ 0 & 0 & 0 & 1 & 0 & 0 & 0 & 0 & 0 \\ 0 & 0 & 0 & 0 & 1 & 0 & 0 & 0 & 0 \\ 0 & 0 & 0 & 0 & 0 & 1 & 0 & 0 & 0 \\ 0 & 0 & -\frac{1}{3} & 0 & 0 & 0 & 1 & 0 & 0 \\ 0 & -\frac{1}{3} & 0 & 0 & 0 & 0 & 0 & 1 & 0 \\ 0 & 0 & 0 & -\frac{1}{3} & 0 & -\frac{1}{3} & 0 & 0 & 1 \end{pmatrix}, \quad (90)$$

$$\mathbf{H}_{D3Q19} = \begin{pmatrix} 1 & 0 & 0 & 0 & 0 & 0 & 0 & 0 & 0 & 0 & 0 & 0 & 0 & 0 & 0 & 0 & 0 & 0 \\ 0 & 1 & 0 & 0 & 0 & 0 & 0 & 0 & 0 & 0 & 0 & 0 & 0 & 0 & 0 & 0 & 0 & 0 \\ 0 & 0 & 1 & 0 & 0 & 0 & 0 & 0 & 0 & 0 & 0 & 0 & 0 & 0 & 0 & 0 & 0 & 0 \\ 0 & 0 & 0 & 1 & 0 & 0 & 0 & 0 & 0 & 0 & 0 & 0 & 0 & 0 & 0 & 0 & 0 & 0 \\ 0 & 0 & 0 & 0 & 1 & 0 & 0 & 0 & 0 & 0 & 0 & 0 & 0 & 0 & 0 & 0 & 0 & 0 \\ 0 & 0 & 0 & 0 & 0 & 1 & 0 & 0 & 0 & 0 & 0 & 0 & 0 & 0 & 0 & 0 & 0 & 0 \\ 0 & 0 & 0 & 0 & 0 & 0 & 1 & 0 & 0 & 0 & 0 & 0 & 0 & 0 & 0 & 0 & 0 & 0 \\ 0 & 0 & 0 & 0 & 0 & 0 & 0 & 1 & 0 & 0 & 0 & 0 & 0 & 0 & 0 & 0 & 0 & 0 \\ 0 & 0 & 0 & 0 & 0 & 0 & 0 & 0 & 1 & 0 & 0 & 0 & 0 & 0 & 0 & 0 & 0 & 0 \\ 0 & 0 & -\frac{1}{3} & 0 & 0 & 0 & 0 & 0 & 0 & 1 & 0 & 0 & 0 & 0 & 0 & 0 & 0 & 0 \\ 0 & 0 & 0 & -\frac{1}{3} & 0 & 0 & 0 & 0 & 0 & 0 & 1 & 0 & 0 & 0 & 0 & 0 & 0 & 0 \\ 0 & -\frac{1}{3} & 0 & 0 & 0 & 0 & 0 & 0 & 0 & 0 & 0 & 1 & 0 & 0 & 0 & 0 & 0 & 0 \\ 0 & -\frac{1}{3} & 0 & 0 & 0 & 0 & 0 & 0 & 0 & 0 & 0 & 0 & 1 & 0 & 0 & 0 & 0 & 0 \\ 0 & 0 & -\frac{1}{3} & 0 & 0 & 0 & 0 & 0 & 0 & 0 & 0 & 0 & 0 & 1 & 0 & 0 & 0 & 0 \\ 0 & 0 & 0 & -\frac{1}{3} & 0 & 0 & 0 & 0 & 0 & 0 & 0 & 0 & 0 & 0 & 1 & 0 & 0 & 0 \\ 0 & 0 & 0 & 0 & -\frac{1}{3} & 0 & 0 & 0 & -\frac{1}{3} & \frac{1}{6} & 0 & 0 & 0 & 0 & 0 & 0 & 1 & 0 \\ 0 & 0 & 0 & 0 & -\frac{1}{3} & 0 & 0 & 0 & \frac{1}{6} & -\frac{1}{3} & 0 & 0 & 0 & 0 & 0 & 0 & 0 & 1 \\ 0 & 0 & 0 & 0 & \frac{1}{6} & 0 & 0 & 0 & -\frac{1}{3} & -\frac{1}{3} & 0 & 0 & 0 & 0 & 0 & 0 & 0 & 0 & 1 \end{pmatrix}, \quad (91)$$

we could obtain the common transformation matrix \mathbf{T} to diagonalize the matrices \mathbf{R} and \mathbf{P} as follows:
in the D2Q9 lattice model,

$$\begin{aligned}\mathbf{TRT}^{-1} &= \mathbf{S}_R = \text{diag}(0, k_1 - k_0, k_1 - k_0, 0, 0, 0, 0, 0, 0), \\ \mathbf{TPT}^{-1} &= \mathbf{S}_P = \text{diag}(0, 0, 0, k_2 - k_0, k_2 - k_0, k_2 - k_0, 0, 0, 0),\end{aligned}\tag{92}$$

in the D3Q19 lattice model,

$$\begin{aligned}\mathbf{TRT}^{-1} &= \mathbf{S}_R = \text{diag}(0, k_1 - k_0, k_1 - k_0, k_1 - k_0, 0, 0, 0, 0, 0, 0, 0, 0, 0, 0, 0, 0, 0, 0, 0), \\ \mathbf{TPT}^{-1} &= \mathbf{S}_P = \text{diag}(0, 0, 0, 0, k_2 - k_0, 0, 0, 0, 0, 0, 0, 0, 0, 0).\end{aligned}\tag{93}$$

Based on Eq. (25), the evolution Eq. (12) can be rewritten as

$$f_i(\mathbf{x} + \mathbf{c}_i \Delta t, t + \Delta t) = f_i(\mathbf{x}, t) - (\mathbf{T}^{-1} \mathbf{S}_f \mathbf{T})_{ij} f_j^{neq} + \Delta t G_i + \Delta t S_i + \frac{\Delta t^2}{2} \bar{D}_i S_i,\tag{94}$$

where \mathbf{S}_f is defined as

$$\text{D2Q9} : \mathbf{S}_f = k_0 \mathbf{I}_{9 \times 9} + \mathbf{S}_R + \mathbf{S}_P = \text{diag}(k_0, k_1, k_1, k_2, k_2, k_2, k_0, k_0, k_0);\tag{95}$$

$$\text{D3Q19} : \mathbf{S}_f = k_0 \mathbf{I}_{19 \times 19} + \mathbf{S}_R + \mathbf{S}_P = \text{diag}(k_0, k_1, k_1, k_1, k_2, k_2, k_2, k_2, k_2, k_2, k_0, k_0, k_0, k_0, k_0, k_0, k_0, k_0, k_0).\tag{96}$$

In addition, for general relaxation parameter blocks \mathbf{K}_1 , \mathbf{K}_2 being off-diagonal matrices as

$$\text{D2Q9} : \mathbf{K}_1 = \begin{pmatrix} k_{1,11} & k_{1,12} \\ k_{1,21} & k_{1,22} \end{pmatrix}, \mathbf{K}_2 = \begin{pmatrix} k_{2,11} & k_{2,12} \\ k_{2,21} & k_{2,22} \end{pmatrix},\tag{97}$$

$$\text{D3Q19} : \mathbf{K}_1 = \begin{pmatrix} k_{1,11} & k_{1,12} & k_{1,13} \\ k_{1,21} & k_{1,22} & k_{1,23} \\ k_{1,31} & k_{1,32} & k_{1,33} \end{pmatrix}, \mathbf{K}_2 = \begin{pmatrix} k_{2,11} & k_{2,12} & k_{2,13} \\ k_{2,21} & k_{2,22} & k_{2,23} \\ k_{2,31} & k_{2,32} & k_{2,33} \end{pmatrix},\tag{98}$$

the relaxation parameter matrix will become a block matrix, and can be given as

$$\text{D2Q9} : \mathbf{S}_f = \begin{pmatrix} k_0 & 0 & 0 & 0 & 0 & 0 & 0 & 0 & 0 \\ 0 & k_{1,11} & k_{1,12} & 0 & 0 & 0 & 0 & 0 & 0 \\ 0 & k_{1,21} & k_{1,22} & 0 & 0 & 0 & 0 & 0 & 0 \\ 0 & 0 & 0 & k_{2,11} & 0 & 0 & 0 & 0 & 0 \\ 0 & 0 & 0 & 0 & \frac{k_{2,12}}{2} + \frac{k_{2,21}}{2} & 0 & 0 & 0 & 0 \\ 0 & 0 & 0 & 0 & 0 & k_{2,22} & 0 & 0 & 0 \\ 0 & 0 & 0 & 0 & 0 & 0 & k_0 & 0 & 0 \\ 0 & 0 & 0 & 0 & 0 & 0 & 0 & k_0 & 0 \\ 0 & 0 & 0 & 0 & 0 & 0 & 0 & 0 & k_0 \end{pmatrix}, \quad (99)$$

D3Q19:

$$\mathbf{S}_f = \begin{pmatrix} k_0 & 0 & 0 & 0 & 0 & 0 & 0 & 0 & 0 & 0 & 0 & 0 & 0 & 0 & 0 & 0 & 0 & 0 & 0 \\ 0 & k_{1,11} & k_{1,12} & k_{1,13} & 0 & 0 & 0 & 0 & 0 & 0 & 0 & 0 & 0 & 0 & 0 & 0 & 0 & 0 & 0 \\ 0 & k_{1,21} & k_{1,22} & k_{1,23} & 0 & 0 & 0 & 0 & 0 & 0 & 0 & 0 & 0 & 0 & 0 & 0 & 0 & 0 & 0 \\ 0 & k_{1,31} & k_{1,32} & k_{1,33} & 0 & 0 & 0 & 0 & 0 & 0 & 0 & 0 & 0 & 0 & 0 & 0 & 0 & 0 & 0 \\ 0 & 0 & 0 & 0 & k_{2,11} & 0 & 0 & 0 & 0 & 0 & 0 & 0 & 0 & 0 & 0 & 0 & 0 & 0 & 0 \\ 0 & 0 & 0 & 0 & 0 & \frac{k_{2,13}}{2} + \frac{k_{2,31}}{2} & 0 & 0 & 0 & 0 & 0 & 0 & 0 & 0 & 0 & 0 & 0 & 0 & 0 \\ 0 & 0 & 0 & 0 & 0 & 0 & \frac{k_{2,12}}{2} + \frac{k_{2,21}}{2} & 0 & 0 & 0 & 0 & 0 & 0 & 0 & 0 & 0 & 0 & 0 & 0 \\ 0 & 0 & 0 & 0 & 0 & 0 & 0 & \frac{k_{2,23}}{2} + \frac{k_{2,32}}{2} & 0 & 0 & 0 & 0 & 0 & 0 & 0 & 0 & 0 & 0 & 0 \\ 0 & 0 & 0 & 0 & 0 & 0 & 0 & 0 & k_{2,22} & 0 & 0 & 0 & 0 & 0 & 0 & 0 & 0 & 0 & 0 \\ 0 & 0 & 0 & 0 & 0 & 0 & 0 & 0 & 0 & k_{2,33} & 0 & 0 & 0 & 0 & 0 & 0 & 0 & 0 & 0 \\ 0 & 0 & 0 & 0 & 0 & 0 & 0 & 0 & 0 & 0 & k_0 & 0 & 0 & 0 & 0 & 0 & 0 & 0 & 0 \\ 0 & 0 & 0 & 0 & 0 & 0 & 0 & 0 & 0 & 0 & 0 & k_0 & 0 & 0 & 0 & 0 & 0 & 0 & 0 \\ 0 & 0 & 0 & 0 & 0 & 0 & 0 & 0 & 0 & 0 & 0 & 0 & k_0 & 0 & 0 & 0 & 0 & 0 & 0 \\ 0 & 0 & 0 & 0 & 0 & 0 & 0 & 0 & 0 & 0 & 0 & 0 & 0 & k_0 & 0 & 0 & 0 & 0 & 0 \\ 0 & 0 & 0 & 0 & 0 & 0 & 0 & 0 & 0 & 0 & 0 & 0 & 0 & 0 & k_0 & 0 & 0 & 0 & 0 \\ 0 & 0 & 0 & 0 & 0 & 0 & 0 & 0 & 0 & 0 & 0 & 0 & 0 & 0 & 0 & k_0 & 0 & 0 & 0 \\ 0 & 0 & 0 & 0 & 0 & 0 & 0 & 0 & 0 & 0 & 0 & 0 & 0 & 0 & 0 & 0 & k_0 & 0 & 0 \\ 0 & 0 & 0 & 0 & 0 & 0 & 0 & 0 & 0 & 0 & 0 & 0 & 0 & 0 & 0 & 0 & 0 & k_0 & 0 \\ 0 & 0 & 0 & 0 & 0 & 0 & 0 & 0 & 0 & 0 & 0 & 0 & 0 & 0 & 0 & 0 & 0 & 0 & k_0 \end{pmatrix}. \quad (100)$$

Finally, based on Eqs.(92), (93), (99), and (100), one can find that \mathbf{S}_f could be partitioned into several relaxation parameter blocks as

$$\mathbf{S}_f = \text{diag}(\mathbf{S}_0, \mathbf{S}_1, \mathbf{S}_2, \dots, \mathbf{S}_m), \quad m < q, \quad (101)$$

where m represents the order of moment, q represents the number of discrete velocities. Moreover, putting the relaxation parameters of zero-order, thirdly-order and higher-order moments together, we could partition the relaxation parameter matrix \mathbf{S}_f into three blocks,

$$\mathbf{S}_f = \text{diag}(\mathbf{S}_0, \mathbf{S}_1, \mathbf{S}_2), \quad (102)$$

where \mathbf{S}_1 , \mathbf{S}_2 , \mathbf{S}_0 , correspond to the first-order, second-order moment and remaining moments of non-equilibrium distribution function, respectively.

8. References

References

- [1] R. Benzi, S. Succi, M. Vergassola, The lattice Boltzmann equation: theory and applications, *Physics Reports* 222 (3) (1992) 145–197.
- [2] S. Chen, G. D. Doolen, Lattice Boltzmann method for fluid flows, *Annual Review of Fluid Mechanics* 30 (1) (1998) 329–364.
- [3] S. Succi, *The lattice Boltzmann equation: for fluid dynamics and beyond*, Oxford University Press, 2001.
- [4] C. K. Aidun, J. R. Clausen, Lattice-Boltzmann Method for Complex Flows, *Annual Review of Fluid Mechanics* 42 (1) (2010) 439–472.
- [5] Z. Guo, C. Shu, *The Lattice Boltzmann Method and its Applications in Engineering*, World Scientific, 2013.
- [6] T. Krüger, H. Kusumaatmaja, A. Kuzmin, O. Shardt, G. Silva, E. M. Viggen, *The Lattice Boltzmann Method: Principles and Practice*, Springer, 2017.
- [7] F. J. Alexander, H. Chen, S. Chen, G. Doolen, Lattice Boltzmann model for compressible fluids, *Physical Review A* 46 (4) (1992) 1967.
- [8] C. Sun, Lattice-Boltzmann models for high speed flows, *Physical Review E* 58 (6) (1998) 7283.
- [9] Y. Gan, A. Xu, G. Zhang, Y. Zhang, S. Succi, Discrete Boltzmann trans-scale modeling of high-speed compressible flows, *Physical Review E* 97 (5) (2018) 053312.
- [10] M. H. Saadat, F. Bösch, I. V. Karlin, Lattice Boltzmann model for compressible flows on standard lattices: Variable Prandtl number and adiabatic exponent, *Physical Review E* 99 (1) (2019) 013306.
- [11] C. Pan, L.-S. Luo, C. T. Miller, An evaluation of lattice Boltzmann schemes for porous medium flow simulation, *Computers & Fluids* 35 (8-9) (2006) 898–909.
- [12] M. Wang, J. He, J. Yu, N. Pan, Lattice Boltzmann modeling of the effective thermal conductivity for fibrous materials, *International Journal of Thermal Sciences* 46 (9) (2007) 848–855.
- [13] Z. Chai, C. Huang, B. Shi, Z. Guo, A comparative study on the lattice Boltzmann models for predicting effective diffusivity of porous media, *International Journal of Heat and Mass Transfer* 98 (2016) 687–696.
- [14] H. Liu, Q. Kang, C. R. Leonardi, S. Schmieschek, A. Narváez, B. D. Jones, J. R. Williams, A. J. Valocchi, J. Harting, Multiphase lattice Boltzmann simulations for porous media applications, *Computational Geosciences* 20 (4) (2016) 777–805.
- [15] Z. Chai, H. Liang, R. Du, B. Shi, A lattice Boltzmann model for two-phase flow in porous media, *SIAM Journal on Scientific Computing* 41 (4) (2019) B746–B772.

- [16] H. Fang, Z. Wang, Z. Lin, M. Liu, Lattice Boltzmann method for simulating the viscous flow in large distensible blood vessels, *Physical Review E* 65 (5) (2002) 051925.
- [17] R. Ouared, B. Chopard, Lattice Boltzmann simulations of blood flow: non-Newtonian rheology and clotting processes, *Journal of Statistical Physics* 121 (1-2) (2005) 209–221.
- [18] J. Zhang, P. C. Johnson, A. S. Popel, An immersed boundary lattice Boltzmann approach to simulate deformable liquid capsules and its application to microscopic blood flows, *Physical Biology* 4 (4) (2007) 285.
- [19] C. Huang, Z. Chai, B. Shi, Non-newtonian effect on hemodynamic characteristics of blood flow in stented cerebral aneurysm, *Communications in Computational Physics* 13 (3) (2013) 916–928.
- [20] X. He, S. Chen, G. D. Doolen, A novel thermal model for the lattice Boltzmann method in incompressible limit, *Journal of Computational Physics* 146 (1) (1998) 282–300.
- [21] Y. Peng, C. Shu, Y. Chew, Simplified thermal lattice Boltzmann model for incompressible thermal flows, *Physical Review E* 68 (2) (2003) 026701.
- [22] Z. Guo, C. Zheng, B. Shi, T. Zhao, Thermal lattice Boltzmann equation for low Mach number flows: decoupling model, *Physical Review E* 75 (3) (2007) 036704.
- [23] N. I. Prasianakis, I. V. Karlin, Lattice Boltzmann method for thermal flow simulation on standard lattices, *Physical Review E* 76 (1) (2007) 016702.
- [24] L. Wang, Y. Zhao, X. Yang, B. Shi, Z. Chai, A lattice Boltzmann analysis of the conjugate natural convection in a square enclosure with a circular cylinder, *Applied Mathematical Modelling* 71 (2019) 31–44.
- [25] Y. Zhao, L. Wang, Z. Chai, B. Shi, Comparative study of natural convection melting inside a cubic cavity using an improved two-relaxation-time lattice Boltzmann model, *International Journal of Heat and Mass Transfer* 143 (2019) 118449.
- [26] X. Shan, G. Doolen, Multicomponent lattice-Boltzmann model with interparticle interaction, *Journal of Statistical Physics* 81 (1-2) (1995) 379–393.
- [27] X. He, X. Shan, G. D. Doolen, Discrete Boltzmann equation model for nonideal gases, *Physical Review E* 57 (1) (1998) R13–R16.
- [28] H. Zheng, C. Shu, Y.-T. Chew, A lattice Boltzmann model for multiphase flows with large density ratio, *Journal of Computational Physics* 218 (1) (2006) 353–371.
- [29] L. Chen, Q. Kang, Y. Mu, Y. He, W. Tao, A critical review of the pseudopotential multiphase lattice Boltzmann model: Methods and applications, *International Journal of Heat and Mass Transfer* 76 (2014) 210–236.
- [30] Y. Zhao, B. Shi, Z. Chai, L. Wang, Lattice Boltzmann simulation of melting in a cubical cavity with a local heat-flux source, *International Journal of Heat and Mass Transfer* 127 (2018) 497–506.
- [31] Z. Chai, D. Sun, H. Wang, B. Shi, A comparative study of local and nonlocal Allen-Cahn equations with mass conservation, *International Journal of Heat and Mass Transfer* 122 (2018) 631–642.
- [32] H. Liang, Y. Li, J. Chen, J. Xu, Axisymmetric lattice Boltzmann model for multiphase flows with large density ratio, *International Journal of Heat and Mass Transfer* 130 (2019) 1189–1205.
- [33] S. Ponce Dawson, S. Chen, G. D. Doolen, Lattice Boltzmann computations for reaction-diffusion equations, *The Journal of Chemical Physics* 98 (2) (1993) 1514–1523.
- [34] D. Wolf-Gladrow, A lattice Boltzmann equation for diffusion, *Journal of statistical physics* 79 (5-6) (1995) 1023–1032.
- [35] X. Yu, B. Shi, A lattice Boltzmann model for reaction dynamical systems with time delay, *Applied Mathematics and Computation* 181 (2) (2006) 958–965.
- [36] C. Huber, B. Chopard, M. Manga, A lattice Boltzmann model for coupled diffusion, *Journal of Computational Physics* 229 (20) (2010) 7956–7976.
- [37] X. He, N. Li, B. Goldstein, Lattice Boltzmann simulation of diffusion-convection systems with surface chemical reaction, *Molecular Simula-*

- tion 25 (3-4) (2000) 145–156.
- [38] B. Shi, Z. Guo, Lattice Boltzmann model for nonlinear convection-diffusion equations, *Physical Review E* 79 (1) (2009) 016701.
- [39] B. Chopard, J. L. Falcone, J. Latt, The lattice Boltzmann advection-diffusion model revisited, *European Physical Journal Special Topics* 171 (1) (2009) 245–249.
- [40] Z. Chai, T. Zhao, Lattice Boltzmann model for the convection-diffusion equation, *Physical Review E* 87 (6) (2013) 063309.
- [41] X. Zhang, A. G. Bengough, J. W. Crawford, I. M. Young, A lattice BGK model for advection and anisotropic dispersion equation, *Advances in Water Resources* 25 (1) (2002) 1–8.
- [42] I. Ginzburg, Equilibrium-type and link-type lattice Boltzmann models for generic advection and anisotropic-dispersion equation, *Advances in Water Resources* 28 (11) (2005) 1171–1195.
- [43] I. Ginzburg, Generic boundary conditions for lattice Boltzmann models and their application to advection and anisotropic dispersion equations, *Advances in Water Resources* 28 (11) (2005) 1196–1216.
- [44] I. Ginzburg, Lattice Boltzmann modeling with discontinuous collision components: Hydrodynamic and Advection-Diffusion Equations, *Journal of Statistical Physics* 126 (1) (2007) 157–206.
- [45] I. Ginzburg, Truncation errors, exact and heuristic stability analysis of two-relaxation-times lattice Boltzmann schemes for anisotropic advection-diffusion equation, *Communications in Computational Physics* 11 (5) (2012) 1439–1502.
- [46] I. Ginzburg, Multiple anisotropic collisions for advection-diffusion Lattice Boltzmann schemes, *Advances in Water Resources* 51 (1) (2013) 381–404.
- [47] H. Yoshida, M. Nagaoka, Multiple-relaxation-time lattice Boltzmann model for the convection and anisotropic diffusion equation, *Journal of Computational Physics* 229 (20) (2010) 7774–7795.
- [48] R. Huang, H. Wu, A modified multiple-relaxation-time lattice Boltzmann model for convection–diffusion equation, *Journal of Computational Physics* 274 (2014) 50–63.
- [49] Z. Chai, B. Shi, Z. Guo, A multiple-relaxation-time lattice Boltzmann model for general nonlinear anisotropic convection–diffusion equations, *Journal of Scientific Computing* 69 (1) (2016) 355–390.
- [50] Z. Chai, B. Shi, L. Zheng, A unified lattice Boltzmann model for some nonlinear partial differential equations, *Chaos, Solitons & Fractals* 36 (4) (2008) 874–882.
- [51] H. Lai, C. Ma, Lattice Boltzmann method for the generalized Kuramoto–Sivashinsky equation, *Physica A: Statistical Mechanics and its Applications* 388 (8) (2009) 1405–1412.
- [52] H. Otomo, B. M. Boghosian, F. Dubois, Efficient lattice Boltzmann models for the Kuramoto–Sivashinsky equation, *Computers & Fluids* 172 (2018) 683–688.
- [53] Z. Chai, N. He, Z. Guo, B. Shi, Lattice Boltzmann model for high-order nonlinear partial differential equations, *Physical Review E* 97 (1) (2018) 013304.
- [54] Z. Guo, C. Zheng, T. S. Zhao, A Lattice BGK Scheme with General Propagation, *Journal of Scientific Computing* 16 (4) (2001) 569–585.
- [55] X. Guo, B. Shi, Z. Chai, General propagation lattice Boltzmann model for nonlinear advection-diffusion equations., *Physical Review E* 97 (4) (2018) 043310.
- [56] X. Xiang, Z. Wang, B. Shi, Modified lattice boltzmann scheme for nonlinear convection diffusion equations, *Communications in Nonlinear Science and Numerical Simulation* 17 (6) (2012) 2415–2425.
- [57] J. Latt, B. Chopard, Lattice Boltzmann method with regularized pre-collision distribution functions, *Mathematics and Computers in Simulation* 72 (2-6) (2006) 165–168.
- [58] R. Zhang, X. Shan, H. Chen, Efficient kinetic method for fluid simulation beyond the Navier-Stokes equation, *Physical Review E* 74 (4) (2006) 046703.
- [59] A. Montessori, G. Falcucci, P. Prestininzi, M. La Rocca, S. Succi, Regularized lattice Bhatnagar-Gross-Krook model for two-and three-

- dimensional cavity flow simulations, *Physical Review E* 89 (5) (2014) 053317.
- [60] K. K. Mattila, P. C. Philippi, L. A. Hegele Jr, High-order regularization in lattice-Boltzmann equations, *Physics of Fluids* 29 (4) (2017) 046103.
- [61] L. Wang, B. Shi, Z. Chai, Regularized lattice Boltzmann model for a class of convection-diffusion equations, *Physical Review E* 92 (4) (2015) 043311.
- [62] L. Wang, Z. Chai, B. Shi, Regularized lattice Boltzmann simulation of double-diffusive convection of power-law nanofluids in rectangular enclosures, *International Journal of Heat and Mass Transfer* 102 (2016) 381–395.
- [63] T. Inamuro, A lattice kinetic scheme for incompressible viscous flows with heat transfer, *Philosophical Transactions of the Royal Society of London A: Mathematical, Physical and Engineering Sciences* 360 (1792) (2002) 477–484.
- [64] T. Inamuro, Lattice Boltzmann methods for viscous fluid flows and for two-phase fluid flows, *Fluid Dynamics Research* 38 (9) (2006) 641.
- [65] Y. Peng, C. Shu, Y. Chew, T. Inamuro, Lattice kinetic scheme for the incompressible viscous thermal flows on arbitrary meshes, *Physical Review E* 69 (1) (2004) 016703.
- [66] M. Yoshino, Y.-h. Hotta, T. Hirozane, M. Endo, A numerical method for incompressible non-Newtonian fluid flows based on the lattice Boltzmann method, *Journal of Non-Newtonian Fluid Mechanics* 147 (1-2) (2007) 69–78.
- [67] T. Nishiyama, T. Inamuro, S. Yasuda, Numerical simulation of the dispersion of aggregated Brownian particles under shear flows, *Computers & Fluids* 86 (2013) 395–404.
- [68] X. Yang, B. Shi, Z. Chai, Generalized modification in the lattice Bhatnagar-Gross-Krook model for incompressible Navier-Stokes equations and convection-diffusion equations, *Physical Review E* 90 (1) (2014) 013309.
- [69] L. Wang, J. Mi, X. Meng, Z. Guo, A localized mass-conserving lattice Boltzmann approach for non-Newtonian fluid flows, *Communications in Computational Physics* 17 (4) (2015) 908–924.
- [70] W. Zhao, L. Wang, W.-A. Yong, On a two-relaxation-time D2Q9 lattice Boltzmann model for the Navier–Stokes equations, *Physica A: Statistical Mechanics and its Applications* 492 (2018) 1570–1580.
- [71] Z. Chai, T. Zhao, Nonequilibrium scheme for computing the flux of the convection-diffusion equation in the framework of the lattice Boltzmann method, *Physical Review E* 90 (1) (2014) 013305.
- [72] L. Wang, W. Zhao, X.-D. Wang, Lattice kinetic scheme for the Navier-Stokes equations coupled with convection-diffusion equations, *Physical Review E* 98 (3) (2018) 033308.
- [73] X. Shan, A central-moment multiple-relaxation-time collision model, arXiv preprint arXiv:1808.04406.
- [74] I. Ginzburg, F. Verhaeghe, D. d’Humières, Two-relaxation-time lattice Boltzmann scheme: About parametrization, velocity, pressure and mixed boundary conditions, *Communications in Computational Physics* 3 (2) (2008) 427–478.
- [75] I. Ginzburg, F. Verhaeghe, D. d’Humières, Study of simple hydrodynamic solutions with the two-relaxation-times lattice Boltzmann scheme, *Communications in Computational Physics* 3 (3) (2008) 519–581.
- [76] S. Cui, N. Hong, B. Shi, Z. Chai, Discrete effect on the halfway bounce-back boundary condition of multiple-relaxation-time lattice Boltzmann model for convection-diffusion equations, *Physical Review E* 93 (4-1) (2016) 043311.
- [77] T. Zhang, B. Shi, Z. Guo, Z. Chai, J. Lu, General bounce-back scheme for concentration boundary condition in the lattice-Boltzmann method, *Physical Review E* 85 (1) (2012) 016701.
- [78] X. He, Q. Zou, L. S. Luo, M. Dembo, Analytic solutions of simple flows and analysis of nonslip boundary conditions for the lattice Boltzmann BGK model, *Journal of Statistical Physics* 87 (1-2) (1997) 115–136.
- [79] A.-M. Wazwaz, The tanh method for generalized forms of nonlinear heat conduction and Burgers–Fisher equations, *Applied Mathematics and Computation* 169 (1) (2005) 321–338.
- [80] P. Lallemand, L.-S. Luo, Theory of the lattice Boltzmann method: Dispersion, dissipation, isotropy, Galilean invariance, and stability, *Physical Review E* 61 (6) (2000) 6546.

- [81] I. V. Karlin, F. Bösch, S. Chikatamarla, Gibbs' principle for the lattice-kinetic theory of fluid dynamics, *Physical Review E* 90 (3) (2014) 031302.

